Transcriptomic Effects of Cannabis-Derived Therapies in a Drosophila model of ALS

Authors and Affiliations

Gurkamal Deol[1†], Ishaan Banwait[1,2†], Steve Campbell[3], Jason R. Gerstner[3,4,5,6,7,8], Kelly Boddington[1,9], Eric Soubeyrand[1,9], José A. Casaretto[1,9], Travis T. Denton[3,4,5*], Akeem Gardner[1*]

[1]Canurta Therapeutics, Mississauga, Ontario, Canada

[2]University of Waterloo, Waterloo, Ontario, Canada

[3]Department of Pharmaceutical Sciences, College of Pharmacy and Pharmaceutical Sciences, Washington State University Health Sciences Spokane, Spokane, Washington, USA

[4]Department of Translational Medicine and Physiology, Elson S. Floyd, College of Medicine, Washington State University Health Sciences Spokane, Spokane, Washington, USA

[5]Steve Gleason Institute for Neuroscience, Washington State University Health Sciences Spokane, Spokane, WA 99202, USA

[6]Sleep and Performance Research Center, Washington State University Health Sciences Spokane, Spokane, Washington, USA

[7]Integrative Physiology and Neuroscience, College of Veterinary Medicine, Pullman, Washington, USA

[8]Voiland School of Chemical Engineering and Bioengineering, Pullman, Washington, USA

[9]University of Guelph, Guelph, Ontario, Canada

[†]These authors contributed equally to this work

[*]Corresponding authors: akeem@canurta.com and travis.denton@wsu.edu

Abstract

Amyotrophic lateral sclerosis (ALS) is a progressive neurodegenerative disease characterized by motor neuron demise, leading to paralysis and death within approximately 3-5 years of symptom onset. Current FDA-approved therapies offer limited disease modification, highlighting the need for treatments that address neuroinflammation and excitotoxicity. Cannabis-derived compounds, particularly flavonoids like Cannflavin A (CFA), have emerged as potential neurotherapeutics due to their anti-inflammatory properties but remain unresearched. In this study, an *in-vivo* C9orf72 *Drosophila melanogaster* model of ALS, expressing toxic poly-GR dipeptide repeats, was used to evaluate the transcriptomic impact of CFA and CNR-401 (a proprietary mixture of flavonoids and terpenes). RNA-sequencing was performed on fly brains followed by differential depression analysis and functional enrichment to identify modulated molecular pathways. Both compounds were found to elicit significant transcriptional remodeling relevant to neurodegenerative pathophysiology. CNR-401 uniquely upregulated ABC transporter genes (NES = 3.17) and fatty acid metabolism (median NES = 2.7515), suggesting a shift toward lipid homeostasis, metabolic resistance, and management of neuroinflammation. CFA treatment primarily enriched gene sets associated with synaptic activity, both excitatory (Glutamatergic Synaptic Transmission NES = 3.165) and inhibitory (GABAergic Synapse NES = 2.175), suggesting a homeostatic stabilization of neurons against excitotoxicity. Both treatments suppressed glucuronidation and xenobiotic metabolism, which may enhance drug bioavailability and support endogenous neuroprotective steroids and coordinated modulation of the circadian clock. In summary, CNR-401 and CFA were shown to be strong therapeutic candidates for ALS patients. Future studies should utilize better controls and mammalian models of ALS to facilitate more accurate ortholog mapping and support gene-level claims.

Introduction

Amyotrophic lateral sclerosis (ALS) is a progressive neurodegenerative disease characterized by demise of upper and lower motor neurons, leading to paralysis and death within approximately 3-5 years of symptom onset (Hardiman et al., 2017). Therapeutic options for ALS remain limited. Riluzole provides a modest survival benefit (Bensimon et al., 1994; R. G. Miller et al., 2012), Edaravone has demonstrated efficacy in a clinically defined subset of patients (Abe et al., 2017), and sodium phenylbutyrate-taurursodiol has shown slower functional decline versus placebo in a randomized trial, while requiring further larger/longer studies (Paganoni et al., 2020). Overall, available therapies provide limited disease modification and no current treatment halts or reverses ALS, underscoring the need for new therapeutic strategies that address its multifactorial pathology (Hardiman et al., 2017). Neuroinflammation has emerged as a significant contributor to ALS progression, yet remains insufficiently addressed by current treatments (Philips & Robberecht, 2011). This has prompted interest in anti-inflammatory and neuroprotective compounds as potential ALS therapeutics.

Compounds derived from *Cannabis sativa* have attracted increasing interest as potential neurotherapeutics due to their diverse bioactive constituents, including cannabinoids as well as flavonoids and terpenes (Bautista et al., 2021; Stasiłowicz-Krzemień et al., 2024). One such molecule is cannflavin A, a prenylated flavone that exhibits anti-inflammatory activity (Abdel-Kader et al., 2023; Bautista et al., 2021). Cannflavin-containing preparations have been reported to suppress pro-inflammatory eicosanoid production via inhibition of microsomal prostaglandin E synthase-1 (mPGES-1) and 5-lipoxygenase (5-LOX) (Werz et al., 2014). In vitro, cannflavin A/B have also been reported to reduce amyloid-β-associated neuronal toxicity

in PC12 cells (Eggers et al., 2019), supporting broader investigation of cannabis-derived flavonoids in neurodegeneration.

In the present study, we focused on two compounds: pure cannflavin A (CFA) and CNR-401, a proprietary mixture of cannabis-derived constituents. CNR-401 is formulated to combine cannflavin A with additional flavonoids and terpenes, with the aim of engaging multiple biological pathways implicated in ALS. However, it remains unclear how treatments like CFA and CNR-401 influence gene expression programs relevant to ALS pathology. Deciphering their transcriptomic impact could clarify which pathways are modulated by these compounds and prioritize mechanisms consistent with neuroprotection.

To address this, we utilized a *Drosophila Melanogaster* model of ALS as an *in vivo* platform for drug evaluation and transcriptomic analysis. The *Drosophila* system offers a short lifespan, well-defined genetics, and powerful tools for targeted transgene expression and genomic analysis (Brand & Perrimon, 1993; Hegde & Srivastava, 2022). *Drosophila* ALS models have yielded insights into conserved disease mechanisms relevant to mammalian neurodegeneration (Hegde & Srivastava, 2022).

Here we employed a transgenic *Drosophila* line modeling C9orf72-associated ALS/FTD, the most common genetic cause of ALS and frontotemporal dementia (DeJesus-Hernandez et al., 2011; Majounie et al., 2012; Renton et al., 2011). In patients, a pathogenic G4C2 hexanucleotide repeat expansion in C9orf72 is linked to ALS/FTD (DeJesus-Hernandez et al., 2011; Renton et al., 2011) and can produce toxic dipeptide repeat (DPR) proteins via repeat-associated non-AUG translation, including arginine-rich DPRs such as poly-glycine-arginine (poly-GR) (Mizielinska et al., 2014). We recapitulated this pathology in flies by pan-neuronal expression of a poly-GR

repeat transgene, which drives neurodegenerative phenotypes *in-vivo* (Mizielinska et al., 2014; Xu & Xu, 2018). This model enables evaluation of how CFA and CNR-401 modulate brain gene expression programs under poly-GR toxicity.

We performed RNA-sequencing of *Drosophila* ALS model brains to capture global gene expression changes induced by CFA and CNR-401. By comparing untreated and treated poly-GR flies, we sought to identify molecular pathways modulated by each compound. We also analyzed male and female flies separately, given evidence that sex influences ALS biology and clinical outcomes (Grassano et al., 2024; Zamani et al., 2024). Our goal was to determine how each compound reshapes the brain transcriptome under poly-GR toxicity and whether these effects differ by sex.

Materials and Methods

Sample Preparation and RNA Sequencing

Drosophila Husbandry and Sample Preparation

Sample preparation including husbandry, treatment, and freezing was conducted in the Washington State University Spokane (WSU Spokane) Drosophila Unified Degeneration Engine (DUDE). Experiments were run using a *Drosophila melanogaster* model of familial ALS (fALS) generated by crossing virgin *elav-Gal4* females obtained from the Bloomington Drosophila Stock Center (Stock number 458) with *UAS-C9orf72*$_{polyGR36}$ males from University College London, Institute of Healthy Ageing. The resulting first filial (F_1) hybrid offspring express the pathogenic dipeptide repeat through the *Gal4/UAS* system.

In each of five crossing vials were placed nine females and three males on normal fly food and kept in a 25 °C day/night incubator. P generation flies were kept in the same vials for 5 days, allowing time for egg laying to occur, before being flipped onto new food. This was repeated to afford two lines of vials capable of producing F_1 generations for the experiments. F_1 generation hybrid flies were collected as they eclosed, separated by gender, and 30 flies were placed into four vials (quadruplicate) per gender (male or female) per food (control or test) for a total of 480 flies per experiment. Two such experiments were conducted: one with test food containing 1.0 mM CFA and another containing 1.0 mM CNR-401. To prevent the flies from getting stuck in the new food, flies were anaesthetised on a CO_2 pad, swept into the food vials held horizontally, and were only returned to a vertical orientation after the flies recovered from sedation.

Industry standard agar-based fly food made onsite at DUDE was used. To prepare the 1.0 mM CFA test food, 45.2 mg CFA (approximately 1035 µL) in excipient, provided by Canurta, was combined with 100.58 g of food and blended completely with an electric mixer. 4-5 g aliquots were dispensed into eight empty fly vials, spun in a centrifuge for 60 sec at 2050 rpm, sealed with cotton Flugs®, and stored at +4 °C. Eight plain food vials were prepared similarly as controls. To prepare the 1.0 mM CNR-401 test food, 393.5 µL of CNR-401, in excipient, was combined with 40.0 g of fly food. Test food preparations were blended completely with an electric mixer, 4-5 g aliquots were dispensed into empty fly vials, spun in a centrifuge at 2050 rpm for 35 sec, sealed with cotton Flugs®, and stored at +4 °C.

F_1 generation flies were kept on food for six days in the 25 °C day/night incubator, observed daily, and any mortality was recorded. On day six, flies were anesthetized on a CO_2 pad, their

heads were removed under magnification, and heads were directly placed into mini-CF, supported in dry ice followed by storage at -80 °C.

RNA Extraction and Sequencing

Extraction and sequencing was performed by National Research Council (NRC) Canada. Extraction was done in eight batches, corresponding to each condition (sex×drug×treatment). RNA from the two male CFA batches (control and treated) was extracted with the Qiagen RNeasy Plus kit on September 4th, 2025 (RIN: 9.3-9.7). Due to the low, but still acceptable, RNA yield (Supplementary Table S1), the NEB Monarch Total RNA prop was employed for all remaining samples on September 11th and 12th, 2025 (RIN: 9.0-9.8). Both kits were used according to manufacturer instructions, with ~100uL of buffer (Qiagen: Buffer RLT+ B-mercaptoethanol, NEB: Protection Buffer) initially added to the tubes containing the flies for ~30 second homogenization with a small pestle, before the remaining buffer volume was added for a final ~10 second homogenization. RNA-seq libraries were prepared using the Illumina Stranded mRNA by Ligation Kit according to manufacturer instructions. Libraries were sequenced on an Illumina Novaseq X+ instrument using v1.5 2x150 bp chemistry. Full extraction and sequencing statistics can be found in Supplementary Tables S1 and S2.

Data Processing and Quality Control

Reads, Alignment, and Quantification

Keeping with best practices for RNA-seq analysis, quality control checks were applied at major steps throughout the analysis (Conesa et al., 2016). Processing of the raw reads to generate counts per gene for each sample was performed by NRC Canada. Quality control for raw reads involved trimming with cutadapt (Martin, 2011) and using Fastqc (Andrews, 2010) to assess the

quality of reads before and after trimming. Alignment and quantification was done with STAR (Dobin et al., 2013; Dobin & Gingeras, 2015) against the BDGP6.46 reference genome (*Drosophila_melanogaster - Ensembl Genome Browser 113*, 2024) in quant mode.

Sample Outlier Detection

After alignment and quantification, data for each sample was parsed and combined into a raw matrix of counts per gene (Supplementary Table S3) and a summary file with quality control metrics for each sample (Supplementary Table S4). This summary file was used for preliminary screening of the samples according to the following thresholds. The sequencing depth, or number of reads for a sample, is important for accurate gene detection and statistical power (Conesa et al., 2016; Dawadi et al., 2025). While the depth of sequencing varies greatly depending on the experiment, 5 million aligned reads is generally considered the absolute minimum (Conesa et al., 2016; *Considerations for RNA Seq Read Length and Coverage | Illumina Knowledge*, 2025). The percentage of mapped reads is an indicator of overall sequencing accuracy and sample quality (Conesa et al., 2016) and is required to be greater than 50% (Dobin & Gingeras, 2015). Ribosomal RNA (rRNA) comprises more than 80% of all RNA molecules in a cell and is purposely depleted during sequencing (O'Neil et al., 2013). Thus, presence of rRNA in the sample is indicative of technical error. The allowable amount of rRNA contamination was capped at 15%, using reads mapping to multiple loci as a proxy for rRNA presence according to the standard set by the alignment tool (Dobin & Gingeras, 2015). Finally, the number of genes detected was measured. This is an experiment-specific metric so sample homogeneity was targeted instead of setting an absolute threshold (Conesa et al., 2016) by excluding samples more than 2 scaled median absolute deviations (MADs) away from the median (Leys et al., 2013; J. Miller, 1991). To further capture technical reproducibility, this relative threshold was then also

applied across the other 3 metrics to detect outlier samples that were more than 2 MADs away from the median in the incorrect direction (i.e. a sample would only be flagged for an abnormally low mapping rate and not for a high one).

To assess samples on a gene-by-gene basis, Cook's distance (Cook, 1977) was calculated for each gene across all samples during processing with DESeq2. In the DEseq2 procedure, samples were flagged as outliers for a gene if their Cook's distance exceeded the 99% confidence boundary for influence (Love et al., 2014). Given the ample replicate size of this study (n=4), a refitting procedure was employed to address these outliers: for any gene containing a flagged outlier, the offending sample was removed for that gene and model parameters were recalculated using the remaining replicates (Love et al., 2014). This gene-specific approach prevents technical artifacts or high biological variance in a single sample from producing false significance for a gene while preserving that sample's valid data points for the rest of the transcriptome.

Manual Verification

Various plots were generated to manually validate quality control practices. Raw counts were filtered to retain only annotated fly genes with ≥ 10 counts and then plotted to assess sequencing quality. Sample quality was assessed by plotting sequencing metrics (Supplementary Figure S1) and the median-of-rations size factors (Supplementary Figure S2). Raw counts were then normalized by dividing by size factors and compressed by $\log_2$(counts) +1 to stabilize variance. Signal uniformity was assessed by boxplots of count distributions (Supplementary Figure S3) and sample clustering was assessed with principal component analysis (PCA) of the first 6 PCs with varying number of genes (all PCAs can be found in Supplementary Figure S4) and sample correlation heatmaps using average hierarchical clustering with a Kendall, Spearman, or Pearson

correlation coefficient as a measure of distance (all three heatmaps can be found in Supplementary Figure S5).

Differential Expression Analysis

Gene Filtering to Boost Power

Following the recommendations of the DESeq2 (Love et al., 2014) vignette, pre-filtering was applied such that genes with less than 10 reads across all samples were dropped in order to reduce the memory size of the data object and increase the speed of count modeling. Genes were also subjected to independent filtering by DESeq2, being removed if the mean normalized count was too low to have any statistical power (Love et al., 2014). Independent filtering was run six times to capture the variability inherent to this statistical process, and a range was presented. This reduces the number of hypothesis tests that need to be performed and mitigates the multiple testing penalty allowing for a greater number of true positives to be detected.

Contrast Definitions

Four experimental questions were investigated: treatment effects, innate sex effects, interactive effects with sex, and the difference in effects between the two drugs. Factor levels were explicitly defined, with female, control, and CFA groups set as reference levels to ensure consistent directionality of the calculated $\log_2$ fold changes. In assessing treatment effects, variance due to sex was subtracted by performing each test on a pooled sex-adjusted group (eg. CFA: treated versus control) and also on each sex-stratified subgroup (eg. CFA females: treated versus control). For innate biological differences between males and females, variation due to treatment was similarly subtracted by testing a pooled group adjusted for treatment (eg. CFA: male versus female) and then looking directly within each treatment-stratified group (eg. CFA

treated: male versus female). A third analysis investigated sex interactions by looking at the difference between how each sex responded to treatment versus control (eg. CFA: male response versus female response) as well as to CNR-401 versus CFA (eg. treated: male difference versus female difference). The fourth analysis explored the effects of the two drugs. Like with analysis one, variance due to sex was first subtracted by performing tests on pooled sex-adjusted groups (eg. treated: CNR-401 versus CFA) and then within sex-stratified subgroups (eg. treated: CNR-401 versus CFA in females). After running all analyses, 22 pairwise comparisons were produced. Full results can be found in Supplementary Table S5.

Statistical Modeling

Counts and metadata were imported and computationally cleaned and validated to ensure compatibility with downstream analysis. Differential expression was analyzed with PyDESeq2 v0.4.9 (Muzellec et al., 2023), a python implementation of the DESeq2 framework (Love et al., 2014). Counts for each gene were modeled using Negative Binomial generalized linear models (GLMs) to accommodate the overdispersion characteristic of RNA-seq data (Conesa et al., 2016). To do this, raw counts for each sample were first normalized using the median-of-ratios method (Love et al., 2014) to estimate sample-specific size factors. This effectively accounts for differences in sequencing depth and allows for fair comparisons between samples. Dispersion was then estimated for each gene using Maximum Likelihood. To improve reliability, these estimates were then moderated by shrinking them towards a global trend line capturing the mean-variance relationship across all genes. Lastly, the size factors and shrunken dispersion estimates were plugged into a GLM for each gene to solve for the coefficients representing $\log_2$ fold changes (LFCs) for each contrast.

Following the fitting of the GLM, statistical significance for each LFC was assessed using Wald tests. This test evaluated the null hypothesis that the LFC for a given contrast is equal to zero, and produced *p*-values accordingly. After *p*-value calculation, LFCs were then shrunk using the bayesian technique *apeglm* to account for the naturally larger LFC in lowly expressed genes (Zhu et al., 2019), improving downstream visualization and ranking.

Significance Filtering

To account for the multiple testing problem resulting from performing thousands of individual Wald tests, *p*-values were adjusted using the Benjamini-Hochberg procedure (Benjamini & Hochberg, 1995). A False Discovery Rate (FDR) threshold of 0.05 was applied, ensuring that proportion of false positives among the rejected null hypotheses was controlled below 5%. Genes were then called significantly differentially expressed if they achieved an adjusted *p*-value (FDR) ≤ 0.05. It was decided that an LFC threshold would not be applied in order to capture the maximum number of DEGs in this exploratory experiment. Results were visualized through volcano and MA plots (Rosati et al., 2024), LFC distributions (Supplementary Figure S6) and cross-comparison plots including a Jaccard overlap heatmap, DEG summary barplot, and venn diagram of DEG overlap.

Functional Analysis

Downstream functional analyses were conducted on the differential expression tables to characterize biological processes, find connections to relevant diseases, and identify potential biomarkers and therapeutic targets.

Gene Enrichment

Permutation-based gene set enrichment analysis (GSEA) was performed on the complete (unfiltered) set of genes using GSEApy v1.1.11 (Fang et al., 2023), implementing the Broad Institute algorithm (Subramanian et al., 2005). Fly genes were first mapped to human orthologs using FlyBase ortholog annotations to leverage comprehensive human pathway databases and then ranked by the DESeq2 Wald statistic (LFC/standard error), which provides a normalized measure of both effect magnitude and statistical confidence. GSEA was conducted with 1000 permutations to establish an empirical null distribution. Gene sets were queried on January 29th 2025 from the following databases: Gene Ontology (Biological Process, Molecular Function, and Cellular Component) (Ashburner et al., 2000; The Gene Ontology Consortium, 2026), KEGG (Kanehisa, 2019; Kanehisa et al., 2025; Kanehisa & Goto, 2000), Reactome (Milacic et al., 2024), and WikiPathways (Agrawal et al., 2024). Pathways with FDR q-value ≤ 0.05 were considered significantly enriched. Complete effects of treatment (CFA or CNR-401 versus control) and sex (male versus female) can be found in Supplementary Tables 6 and 7, respectively.

Protein Network Interactions

To elucidate the functional organization of differentially expressed genes and identify regulatory hubs, protein-protein interaction (PPI) networks were constructed using STRING (v11.5) (Szklarczyk et al., 2023). For each of the 22 comparisons, significant DEGs (FDR ≤ 0.05) were submitted to STRING with *D. melanogaster* as the reference organism, and networks were built using high-confidence interactions (combined score ≥ 0.400) spanning experimental, co-expression, and text-mining evidence channels. DEGs were limited to the top 200 per comparison due to API constraints. Network topology was quantified in NetworkX (v2.6.0) and

hub genes were defined using a composite score integrating degree centrality, betweenness centrality, closeness centrality, eigenvector centrality, and PageRank. Functional modules were detected via Louvain clustering. A cross-comparison analysis was then performed to identify recurrent hub genes (Supplementary Table S8). Network statistics can be found in Supplementary Table S9.

Systems Biology Analysis

To complement differential expression testing and identify co-expressed gene programs associated with experimental factors, weighted gene co-expression network analysis (WGCNA) was performed across all 32 samples (Langfelder & Horvath, 2008). This unsupervised framework grouped genes into modules based on expression-pattern similarity, enabling detection of coordinated programs that may not be recovered by pairwise contrasts. Networks were built from a variance-stabilized ($\log_2$+1) expression matrix comprising 4,989 genes after low-variance filtering (top 50% most variable genes capped at 5000 for computational efficiency), using a soft-thresholding power of $\beta = 3$ selected to achieve scale-free topology fit ($R^2 = 0.87$) with mean connectivity of 205. Modules were detected by hierarchical clustering with dynamic tree cutting (minimum module size 30 genes), and closely related modules were merged at an eigengene correlation threshold of 0.75 (Supplementary Table S2). Trait correlations can be found at Supplementary Table 10 and are visualized in Supplementary Figure 7. Hub genes for each module are listed in Supplementary Table S11.

Results

Quality Control and Sample Assessment

Sequencing quality and preliminary sample screening

RNA-seq produced ~1.1 billion reads across 32 samples. Uniquely mapped reads per sample (sequencing depth) ranged from 8.90-45.3 million (median 23.0 million), surpassing the threshold of 5 million reads. The percentage of these reads that mapped to the *D. melanogaster* reference genome (BDGP6.46) was 63.7-75.8% (median 73.2%), well above the threshold of 50%. Reads that mapped to multiple loci accounted for 0.88-2.52% (median 1.11%) of the total reads. This is below the 15% threshold for rRNA contamination. Gene detection was consistent, with 12,940-16,396 genes detected per sample (median 14,578.5). Results are visualized in Supplementary Figure S1. While all samples were above absolute thresholds, a few samples were flagged for deviating from the median. Two samples were below 2 MADs of the median for mapping rate (64.3% and 63.7%). In addition, four samples were above 2 MADs of the median for rRNA content (1.7%, 1.8%, 2.5%, and 1.6%). Replicate 1 of the male control in the CFA group stood out as a sample that was flagged for both abnormally low gene detection (12940) and high rRNA content (1.5%). All seven outlier samples were flagged before proceeding to further processing and can be found listed in Supplementary Table S4.

DESeq2 size factors (median-of-ratios) ranged from 0.52-1.88 (plotted in Supplementary Figure S2), indicating moderate depth/complexity variation without evidence of major technical failure: there were no extreme size factors >3.0 or <0.3.

Sample clustering identifies validates the main sources of variation

After variance-stabilizing the counts, PCA of samples revealed sex and drug as top sources of variation (PC1 and PC3, respectively, in Figure 1). Treatment (treated versus control) was not found to separate on any of the first 6 PCs, cumulatively representing 50.2 of variance (Supplementary Figure S4). Results remained the same with PCA of only the top 500 and 1000

most-variable genes (Supplementary Figure S4). This aligns with the expectation for PCs to explain covariates like sex and drug but not predict response variables such as treatment (Ma & Dai, 2011).

Figure 1. Principal component analysis of normalized gene expression.

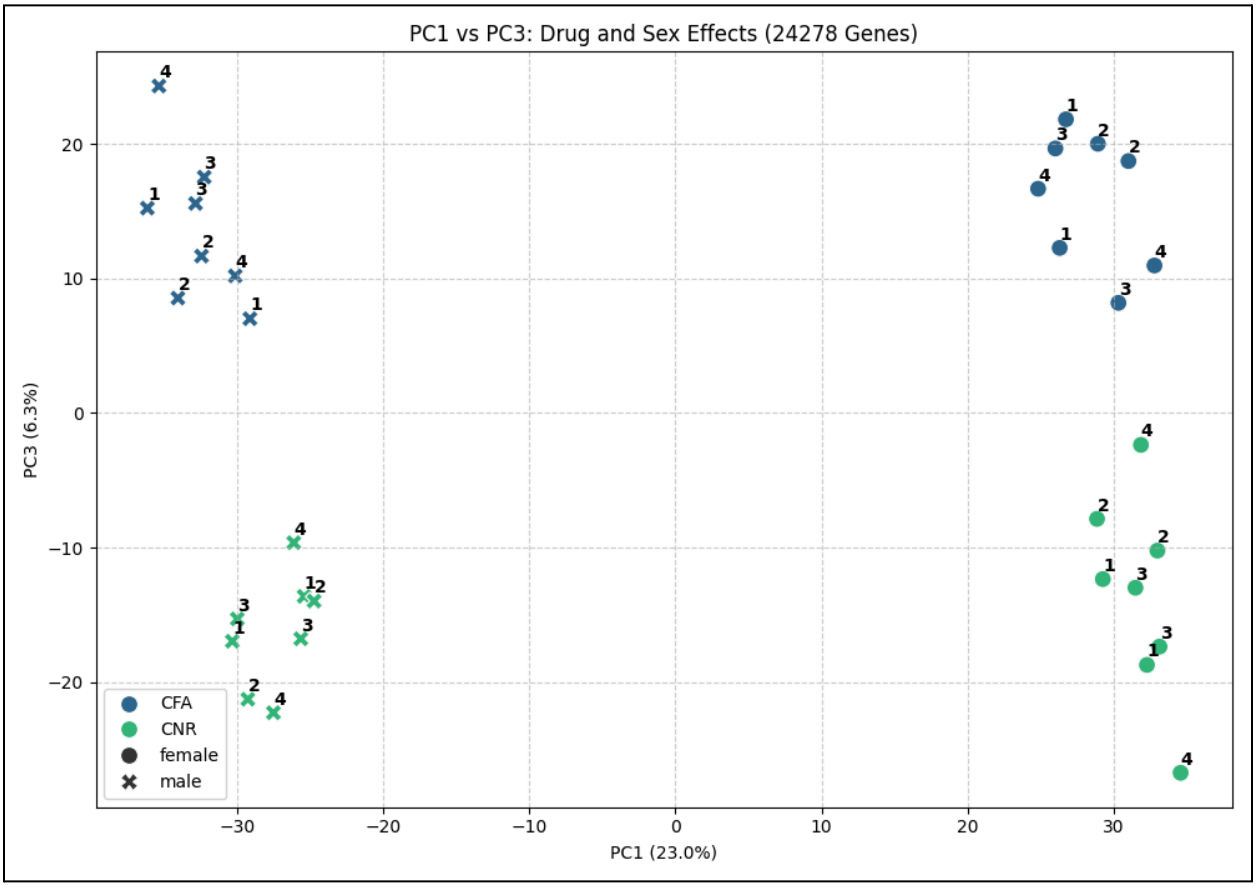

PCA of 32 RNA-seq samples using all genes after size-factor normalization and $\log_2$+1 shrinkage. Sex very clearly separated on PC1 (23.0% variance) with males as crosses on the left and females as circles on the right. Choice of drug separated more subtly on PC3 (6.3% variance) with CFA in blue near the top and CNR-401 in green near the bottom.

Clustering sample gene expression profiles by similarity (Figure 2) supported the patterns revealed by the PCA, with samples first grouping by sex, and then by compound. Distinctly, treatment effects were captured as a more-subtle tertiary source of variation. The fact that control samples cluster first by drug revealed the presence of strong batch effects which were kept in mind for later interpretations. Heatmaps calculated with alternative correlation coefficients can be found in Supplementary Figure S5.

Figure 2. Sample-to-sample distance matrix with hierarchical clustering.

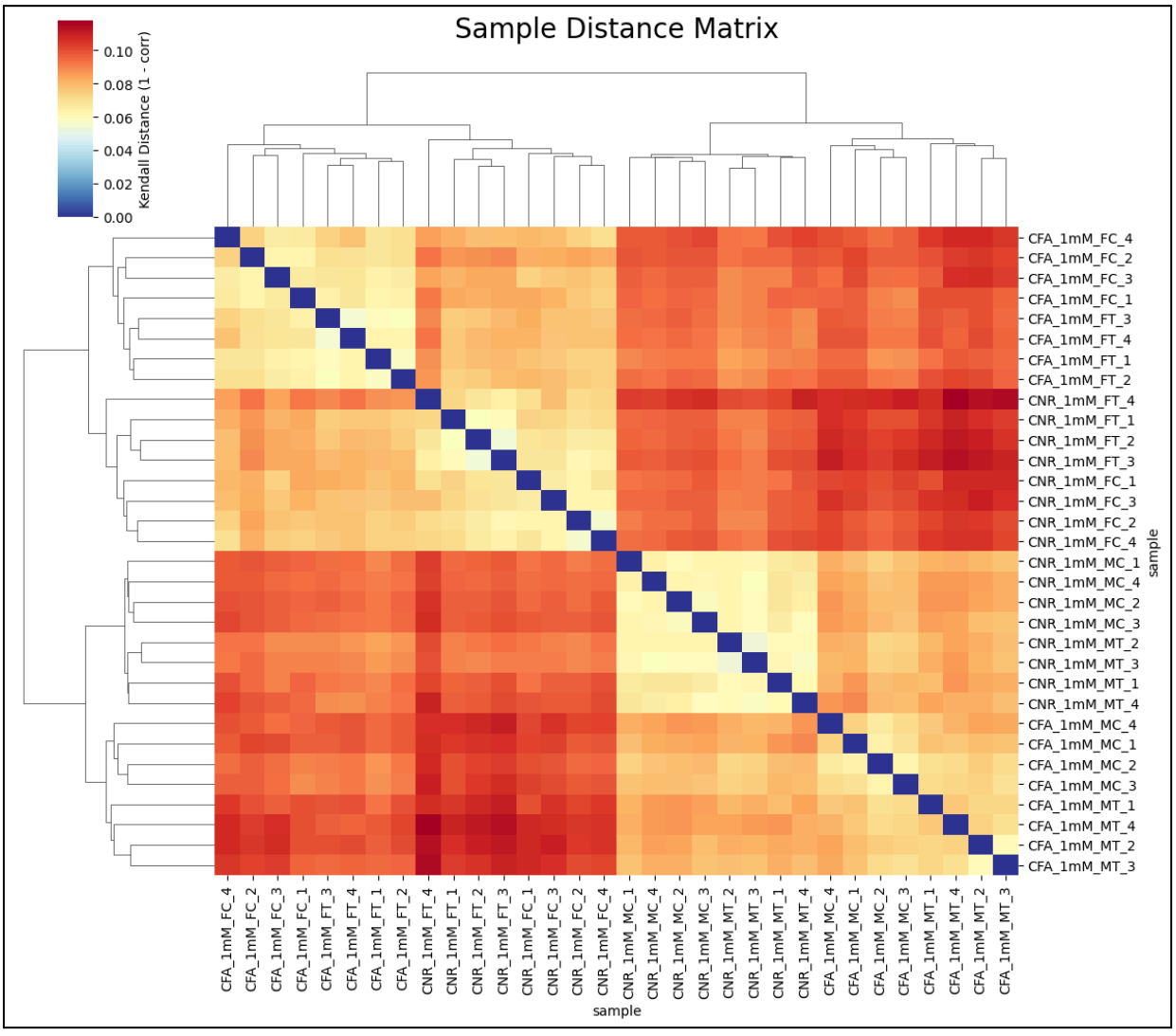

Kendall distances (1 - correlation) between samples computed from variance-stabilized (log_2+1) expression values of flybase genes with >10 counts. Hierarchical clustering (average method) reveals primary grouping by sex, secondary grouping by compound (CFA vs CNR-401), and tertiary grouping by treatment. Color warmness reflects distance (more red=more distance=less similar).

Sensitivity analysis and QC summary

To quantify impact, plots were regenerated after removing outliers. While clustering was slightly improved, core signals were retained. Therefore, all 32 samples were kept for primary analyses to maximize power, with DESeq2 Cook's distance filtering providing additional gene-level protection. Overall QC supported proceeding with differential expression analysis: sequencing depth and mapping were acceptable, samples clustered by sex and drug covariates, as well as by the primary treatment variable, validating the experimental procedure. The strong batch effects, revealed through the clustering of control samples, indicated that pre-existing biological variability was greater than treatment effects and thus cross-experiment comparisons must be interpreted with caution (i.e. CFA-treated samples cannot simply be compared to CNR-401-treated samples).

Differential expression landscape

Across all comparisons, significant DEGs ranged from 108 to 6,133 (Figure 4). Of the 55,508 total DEGs, 16,836 were retained after pre-filtering out genes with less than 10 reads across all samples, and 13,776-13,804 genes passed independent filtering from DESeq2, reflecting adequate expression for model fitting. Primary treatment contrasts identified robust transcriptional responses for both compounds, with larger effects for CFA than CNR-401 in

sex-adjusted analyses (CFA: 1,275 DEGs; 600 up, 675 down; CNR-401: 734 DEGs; 394 up, 340 down). Sex-stratified contrasts showed marked sex dependence: CFA responses were stronger in males than females (736 versus 361 DEGs), whereas CNR-401 responses were stronger in females than males (907 versus 235 DEGs), indicating sexually dimorphic treatment programs.

Figure 4. Differentially expressed genes across 22 comparisons.

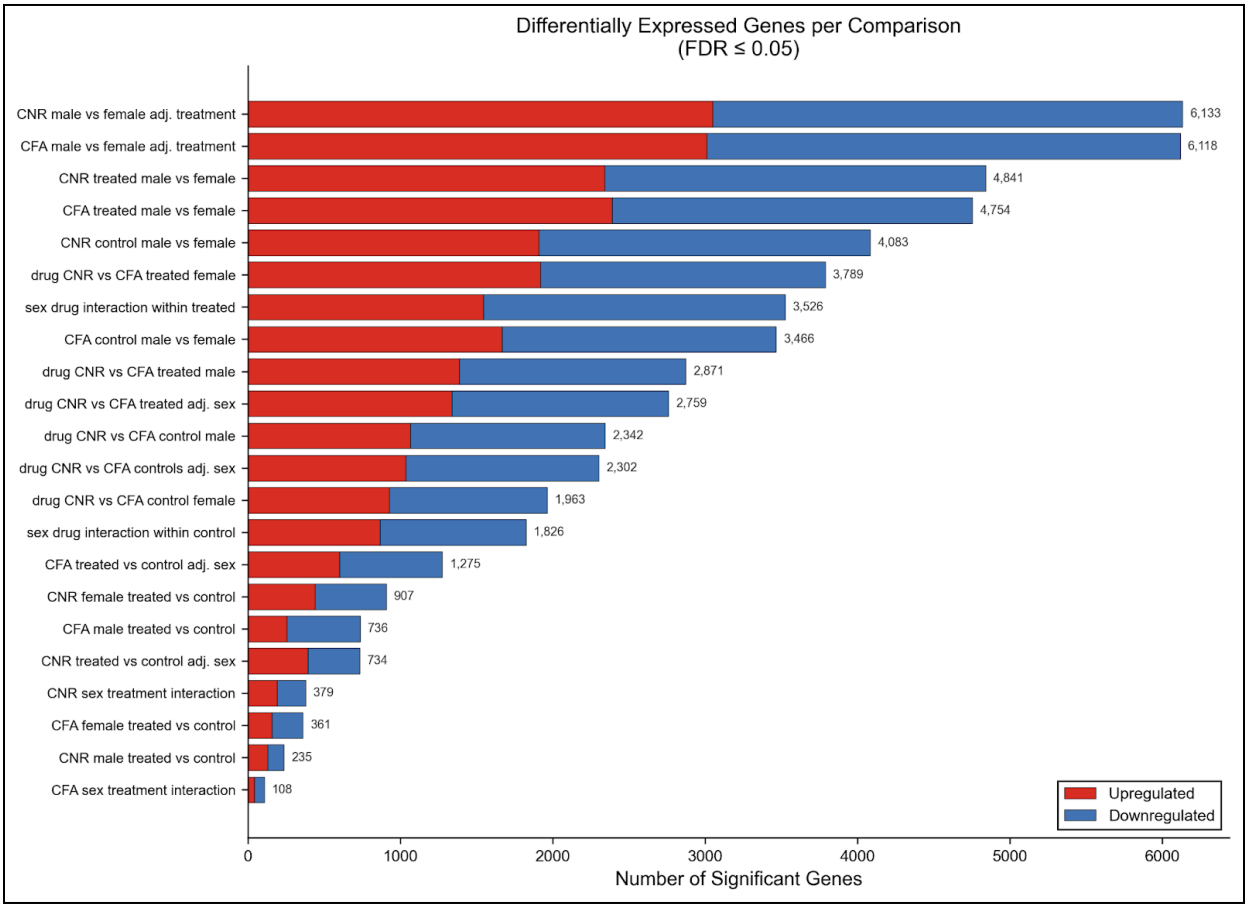

Stacked bar chart showing the unfiltered number of upregulated (red) and downregulated (blue) genes for each comparison at FDR ≤ 0.05. Sex differences accounted for the largest number of DEGs. Values indicate total DEG count.

Sex effects dominated the transcriptome. Treatment-adjusted male versus female comparisons yielded 6,118 DEGs for CFA and 6,133 for CNR-401 (~37% of tested genes), consistent with pervasive sex-biased expression in D. melanogaster (Graveley et al., 2011; Parisi et al., 2003) and the sex-driven separation observed in PCA. Sex×treatment interaction testing identified a smaller but significant set of genes with sex-dependent treatment responses in both experiments (CFA: 108 DEGs; CNR-401: 379 DEGs), with CNR-401 exhibiting a larger interaction component. Exploratory compound comparisons (CNR-401 versus CFA) produced thousands of DEGs across matched conditions (sex-adjusted treated: 2,759; sex-adjusted control: 2,302; with larger differences in sex-stratified contrasts), but these results must be interpreted cautiously because CFA and CNR-401 were administered in separate cohorts rather than a paired design, and batch effects were strong (see Sensitivity analysis and QC summary).

Overlap analysis using Jaccard similarity (Figure 5) indicated substantial concordance among sex-effect DEG sets (Jaccard >0.5), moderate overlap among within-compound treatment contrasts (~30-40%), and low overlap between treatment and sex DEG sets (<15%), supporting largely distinct programs. Interaction DEG sets were minimally shared between compounds (Jaccard = 0.12), consistent with compound-specific patterns of sex-dependent response. A focused Venn analysis of key contrasts similarly supported separation between sex- and treatment-associated gene sets, with a small shared subset (Figure 6D). Log_2 fold-change distributions were consistent with effect magnitude differences (Supplementary Figure S6): treatment contrasts showed modest median absolute effects (|LFC| ~0.4-0.8) with broadly balanced up- and down-regulation, whereas sex contrasts exhibited wider distributions including strongly sex-biased genes (|LFC| > 4). Collectively, these results show that both compounds elicit

significant transcriptional remodeling (stronger for CFA in pooled analyses), sex is the dominant axis of variation, and treatment responses include a measurable sex-dependent component, motivating downstream functional enrichment to resolve affected pathways and biological processes.

Figure 5. Jaccard similarity of DEG sets across comparisons.

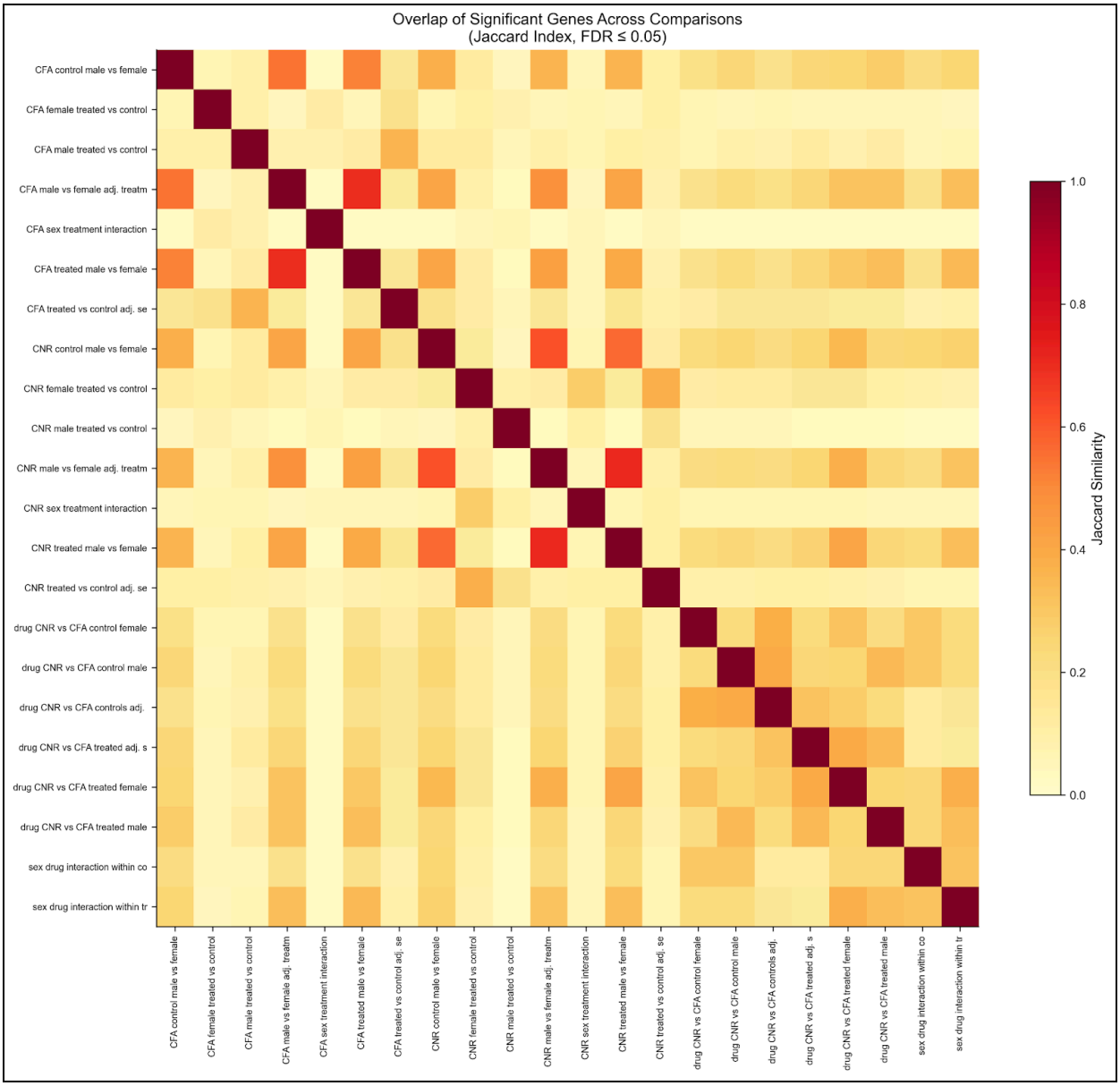

Heatmap showing pairwise Jaccard index (intersection/union) between filtered significant genes from all 22 comparisons. Sex-effect comparisons cluster together (Jaccard > 0.5, warm colors). Treatment-effect comparisons show moderate overlap (~0.3-0.4). Treatment and sex gene sets show minimal overlap (<0.15), indicating largely distinct transcriptional programs.

Figure 6. Overlap of differentially expressed genes between treatment and sex comparisons.

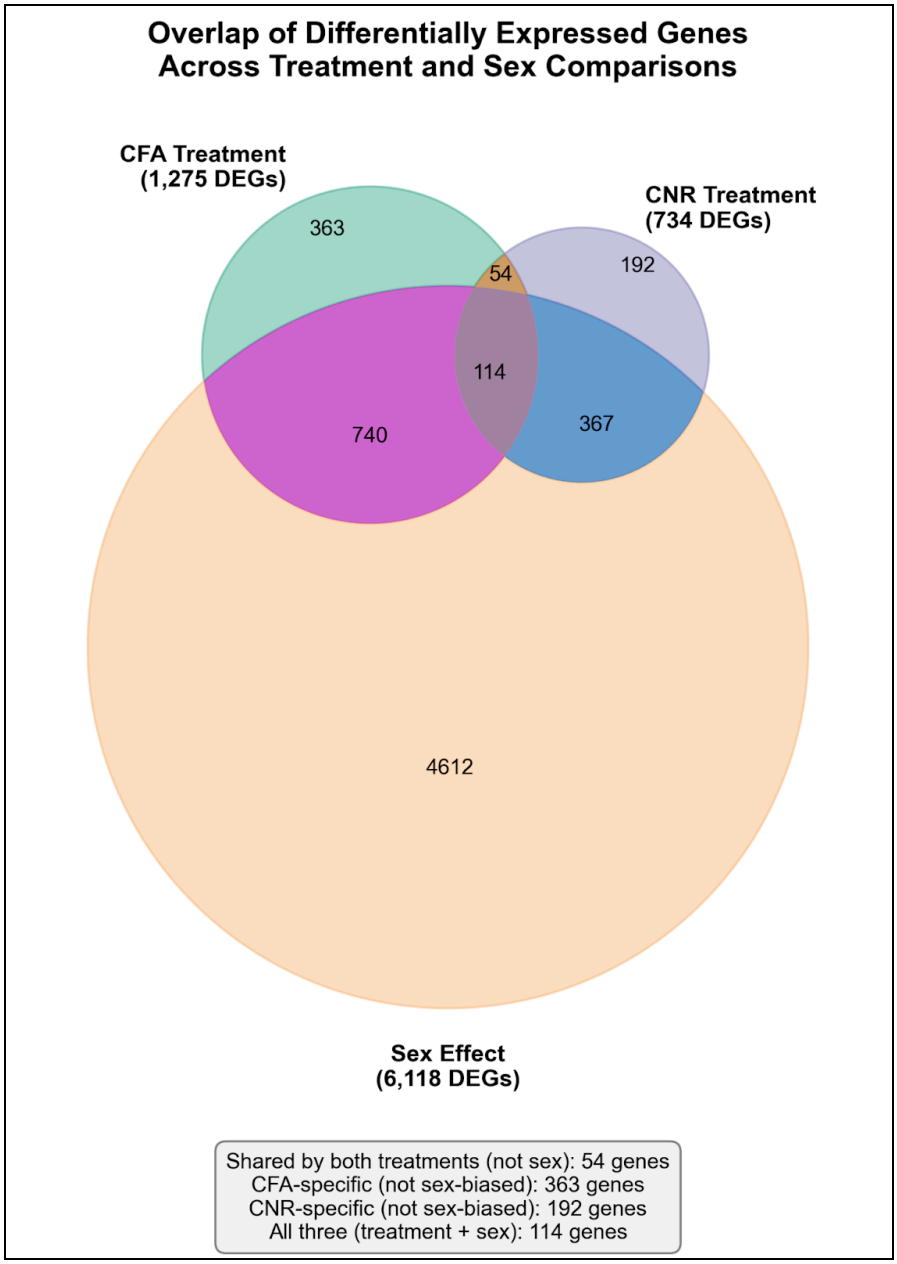

Three-way Venn diagram showing overlap between filtered CFA treatment DEGs (1,275 genes, teal), CNR-401 treatment DEGs (734 genes, purple), and sex-effect DEGs (6,118 genes, orange). Treatment effects show substantial overlap with each other but minimal overlap with sex-biased genes, indicating largely distinct transcriptional programs. Inset box shows key statistics.

Treatment effects - CFA and CNR-401 transcriptional responses

Both CFA and CNR-401 induced differential gene expression in *D. melanogaster* (Table 1; Fig. 1). In sex-adjusted models, CFA produced 1,275 DEGs and CNR-401 produced 734 DEGs (FDR ≤ 0.05), with bidirectional changes in both compounds. Sex-stratified analyses revealed pronounced sexual dimorphism: CFA showed male-biased responsiveness (735 versus 363 DEGs), whereas CNR-401 showed female-biased responsiveness (907 versus 236 DEGs).

Table 1. Differential expression summary: treatment effects.

DEGs: FDR ≤ 0.05. Genes subjected to filtering.

Contrast	N tested	N DEGs	Up	Down
CFA treated vs control (sex-adjusted)	10,008	1,275	600	675
CNR-401 treated vs control (sex-adjusted)	9,995	734	394	340
CFA females vs control	10,316	363	159	204
CFA males vs control	9,534	735	256	479
CNR-401 females vs control	10,239	907	441	466

CNR-401 males vs control	9,343	236	131	105

CFA and CNR-401 shared 317 DEGs, including timeless (down) and *CG10550* (up), indicating common circadian-related targets (Table 2). CFA-specific responses included downregulation of heat shock proteins (*Hsp23, Hsp26, Hsp27*) and upregulation of spo (ecdysone biosynthesis). CNR-401-specific responses included upregulation of metabolic genes *(Pepck1, Cyp6a2*) and downregulation of immune genes (*CecB*) (Larkin et al., 2021)].

Table 2. Conserved and compound-specific treatment-responsive genes.

Class	**Genes**	**Direction**	**CFA LFC**	**CNR-401 LFC**
Shared	*tim*	Down	−1.17	−1.13
	l(2)efl	Down	−1.89	−1.10
	CG10550	Up	+1.36	+1.72
CFA-specific	*Hsp23, Hsp26, Hsp27*	Down	−1.0 to −1.2	—
	spo	Up	+1.04	—

CNR-401 -specific	*Pepck1*	Up	—	+0.87
	CecB	Down	—	−1.38

Figure 7. Volcano plots of treatment effects.

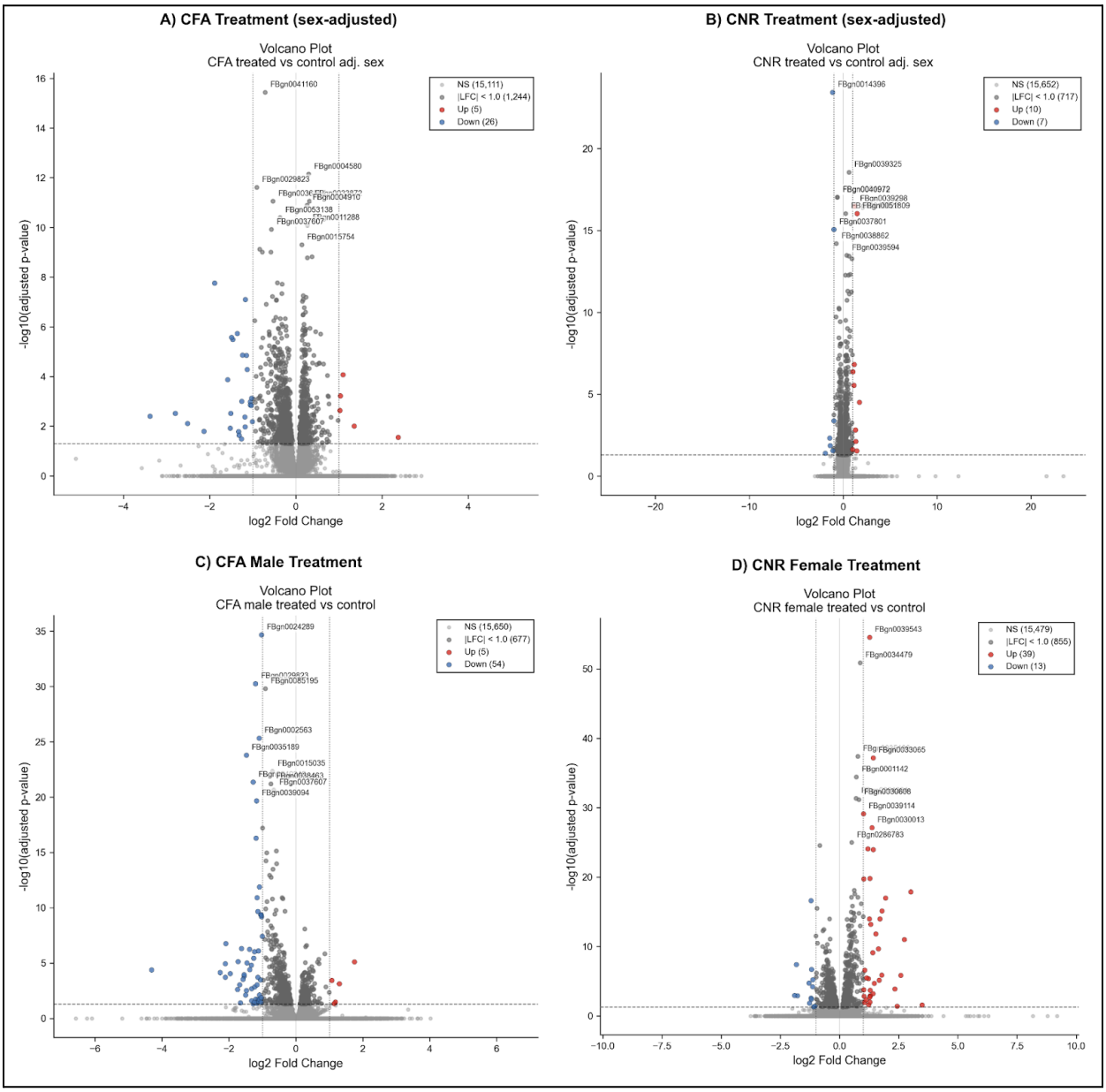

Log_2 fold-change vs $-log_{10}$(adjusted p-value). Dashed lines: FDR = 0.05. (A) CFA sex-adjusted (1,275 DEGs). (B) CNR-401 sex-adjusted (734 DEGs). (C) CFA males (735 DEGs). (D) CNR-401 females (907 DEGs).

Sex effects and sex×treatment interactions

Sex differences dominated the transcriptome across conditions (Table 3; Fig. 3). In treatment-adjusted models, 6,100 genes (37% of tested) showed significant sex-biased expression, with balanced male- versus female-biased counts and similar effect magnitudes for both compounds (median |LFC| ~1.15 among significant genes). Sex×treatment interaction tests identified genes with sex-dependent treatment responses: 108 for CFA and 380 for CNR-401 (Table 3).

Table 3. Sex effects and sex×treatment interactions.

Positive interaction LFC indicates larger treatment effect in males than females (difference-in-differences). DEGs: FDR ≤ 0.05. Genes subjected to filtering.

Contrast	N tested	N DEGs	Male-biased	Female-biased
Sex main effect (treatment-adjusted)				
CFA male vs female	13,804	6,119	3,012	3,107
CNR-401 male vs female	13,776	6,135	3,051	3,084

Sex effect within condition				
CFA treated	12,183	4,754	2,389	2,365
CFA control	11,850	3,466	1,666	1,800
CNR-401 treated	12,183	4,842	2,339	2,503
CNR-401 control	11,489	4,083	1,907	2,176
Sex×treatment interaction			**Male-stronger**	**Female-stronger**
CFA interaction	10,013	108	41	67
CNR-401 interaction	9,679	380	192	188

Male-biased genes included immune peptides such as Cecropins (*CecA1, CecA2, CecB*) and Attacins (*AttA, AttB*), consistent with known sex differences in immune gene expression in *D. melanogaster*. Female-biased genes included heat shock proteins (*Hsp23, Hsp26, Hsp27*) and circadian regulators.

Sex×treatment interaction analysis identified genes whose treatment response differed between sexes. CFA showed 108 interaction genes while CNR-401 showed 380, with CNR-401 exhibiting a larger sex-dependent component.

Figure 8. Volcano plots of sex effects and sex×treatment interactions.

(A-B) Volcano plots for male vs. female contrasts (treatment-adjusted) in CFA (6,118 DEGs) and CNR-401 (6,133 DEGs). Positive LFC indicates male-biased expression. Male-biased genes include immune peptides (CecB, AttA); female-biased genes show higher heat shock protein expression. (C) CFA sex×treatment interaction (108 DEGs): genes whose treatment response differs between sexes. Gnmt shows strong female-biased treatment response (interaction LFC = −3.99). (D) CNR-401 sex×treatment interaction (379 DEGs): 3.5× more interaction genes than CFA, indicating more sex-specific effects.

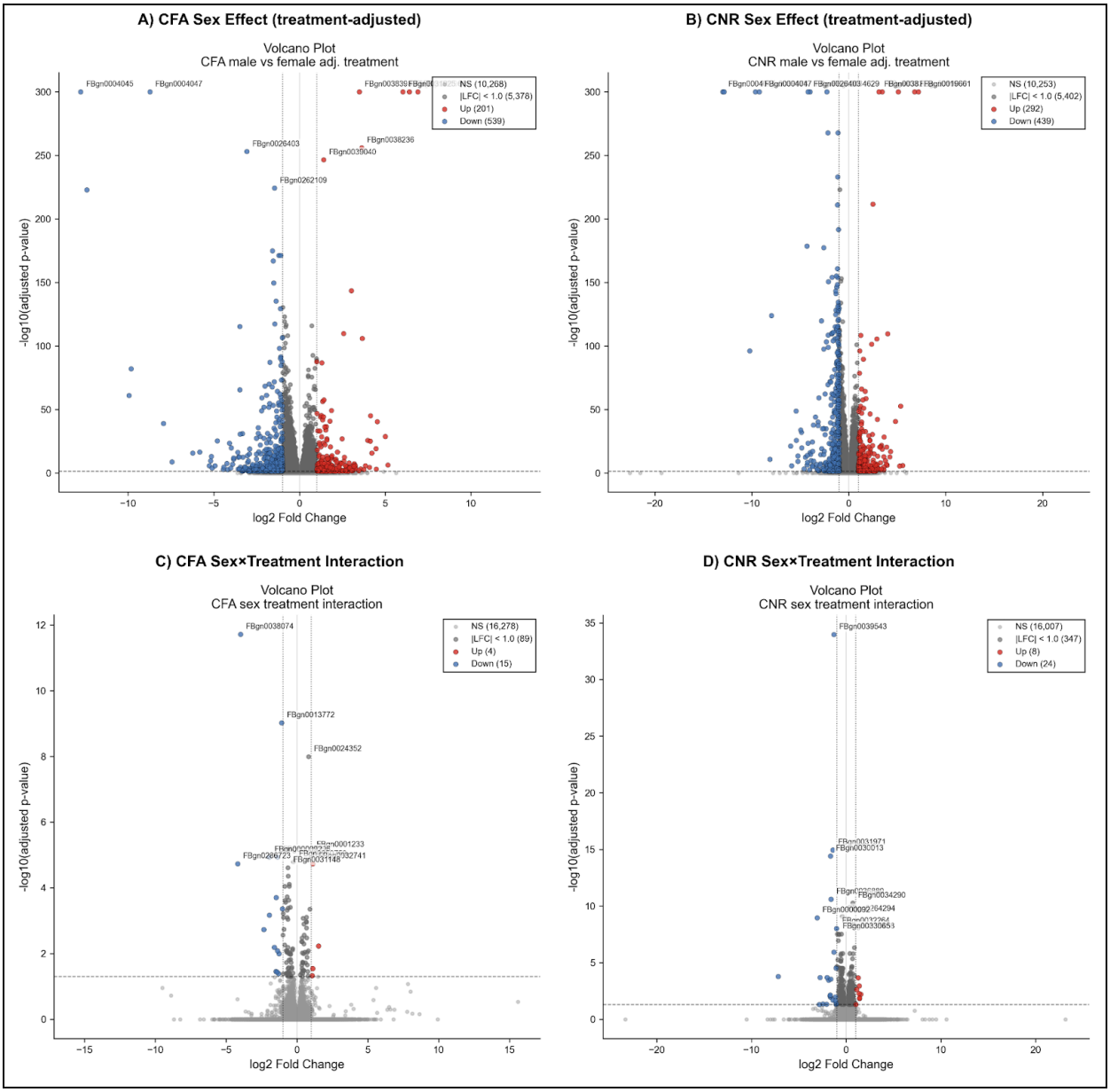

Functional enrichment analysis

To characterize the biological processes underlying differential expression, we performed gene set enrichment analysis (GSEA) using a permutation-based approach with 1,000 permutations. Genes were mapped to human orthologs and ranked by their Wald statistic prior to GSEA against

GO (Biological Process, Molecular Function, Cellular Component), KEGG, Reactome, and WikiPathways databases.

Treatment-associated pathway signatures

GSEA identified 858 and 434 significantly enriched pathways (FDR ≤ 0.05) for CFA and CNR-401 treatment effects, respectively (Supplementary Table S6). CFA treatment showed strong enrichment for neuronal signaling pathways, including potassium channel activity (NES = 3.17, FDR < 0.001), glutamatergic synaptic transmission (NES=3.02, FDR < 0.001), and synaptic vesicle cycle (NES = 2.90, FDR < 0.001). CNR-401 treatment showed robust enrichment for ABC transporters (NES = 3.17, FDR < 0.001), cytochrome P450 oxidation (NES = 3.00, FDR < 0.001), and fatty acid metabolism (NES = 2.88, FDR < 0.001).

Pathways downregulated by both treatments showed convergent themes in xenobiotic metabolism and glucuronidation. CFA treatment suppressed drug metabolism pathways (NES = −3.21, FDR < 0.001), pentose and glucuronate interconversions (NES = −3.24, FDR < 0.001), and biological oxidations (NES = −3.07, FDR < 0.001). Similarly, CNR-401 treatment suppressed glucuronidation (NES = −3.07, FDR < 0.001), pentose/glucuronate interconversions (NES = −3.01, FDR < 0.001), and ascorbate/aldarate metabolism (NES = −2.96, FDR < 0.001).

Table 4. Top GSEA enrichments for treatment effects

The top 5 upregulated and downregulated pathways enriched in CNR-401 treatment, CFA treatment, and both treatments, ranked by absolute NES. NES = normalized enrichment score; positive NES indicates pathway upregulated by treatment; negative NES indicates pathway

downregulated by treatment; NES range captures the range of scores for the 5 pathways. Full results in Supplementary Table S6.

Compound	Direction	Top enriched pathways	NES range	FDR range
CFA	Up	Potassium channel activity, potassium ion transmembrane transport, glutamatergic synaptic transmission, synaptic vesicle cycle, monoatomic cation transport	2.89 – 3.17	< 0.001
CFA	Down	Biotransformation Phase I/II, pentose and glucuronate interconversions, xenobiotic metabolism by cytochrome P450, retinol metabolism, glucuronidation	−3.28 – −3.05	< 0.001
CNR-401	Up	ABC transporters, cytochrome P450 oxidation, long-chain fatty acid metabolism, monocarboxylic acid transport, very long-chain fatty acid metabolism	2.71 – 3.17	< 0.001
CNR-401	Down	Glucuronidation, pentose and glucuronate interconversions, ascorbate and aldarate metabolism, glucuronate metabolism, porphyrin metabolism	−3.07 – −2.82	< 0.001

Both	Up	Ribonucleoprotein complex biogenesis, G-protein-coupled receptor signaling, translation initiation factor activity, cyclic nucleotide binding	1.63 – 2.34	< 0.05
Both	Down	Mucin-type O-glycan biosynthesis, O-glycan processing, lysosomal lumen, retinoid metabolism, drug metabolism	−2.45 – −1.72	< 0.05

GSEA using the full ranked transcriptome identified coordinated pathway shifts not captured by thresholded DEG sets (Table 5). CFA treatment was associated with strong enrichment for synaptic function, including glutamatergic synaptic transmission (GO:0035249; FDR < 0.001; 58% tag), synaptic vesicle cycle (KEGG; FDR < 0.001; 52% tag), and potassium ion transmembrane transport (GO:0071805; FDR < 0.001; 58% tag). CNR-401 treatment showed pronounced enrichment for metabolic transport processes, with ABC transporters (KEGG; FDR < 0.001; 45% tag) and monocarboxylic acid transport (GO:0015718; FDR < 0.001; 48% tag) among the top terms. Both treatments showed convergent downregulation of glucuronidation (Reactome; FDR < 0.001) and pentose/glucuronate interconversions (KEGG; FDR < 0.001) (Supplementary Table S6).

Table 5. Top GSEA enrichments across treatment comparisons

GSEA performed with gseapy using genes ranked by Wald statistic. FDR q-values reported. Tag % indicates percentage of leading-edge genes out of the gene set.

Comparison	Gene set	GO/Pathway ID	FDR q	Tag %
CFA treated vs control	Potassium channel activity	GO:0005267	< 0.001	58%
CFA treated vs control	Glutamatergic synaptic transmission	GO:0035249	< 0.001	58%
CFA treated vs control	Synaptic vesicle cycle	KEGG	< 0.001	52%
CFA treated vs control	Monoatomic cation transmembrane transport	GO:0098655	< 0.001	55%
CNR-401 treated vs control	ABC transporters	KEGG	< 0.001	45%
CNR-401 treated vs control	Cytochrome P450 oxidation	WikiPathways	< 0.001	62%
CNR-401 treated vs control	Long-chain fatty acid metabolism	GO:0001676	< 0.001	51%
CNR-401 treated vs control	Fatty acid metabolic process	GO:0006631	< 0.001	48%

Sex-biased pathway enrichments

Sex-effect enrichments were highly consistent between CFA and CNR-401 treatment backgrounds (Supplementary Table S7). Male-biased genes (positive NES; 226 pathways in CFA, 262 in CNR-40) were enriched for xenobiotic metabolism, including Phase I functionalization of compounds (NES = 3.08, FDR < 0.001), biological oxidations (NES = 3.07, FDR < 0.001), and biotransformation Phase I/II (NES = 3.05–3.21, FDR < 0.001). Male-biased enrichment was also observed for amino acid transport (GO:0006865; NES = 2.80–2.94, FDR < 0.001) and glucuronidation (NES = 2.80–2.90, FDR < 0.001).

Female-biased genes (negative NES; 255 pathways in CFA, 107 in CNR-401) were enriched for translation machinery and ribosome biogenesis. The strongest female-biased enrichments included eukaryotic translation elongation (NES = −3.51, FDR < 0.001), peptide chain elongation (NES = −3.49, FDR < 0.001), SRP-dependent cotranslational protein targeting (NES = −3.49, FDR < 0.001), and cytoplasmic ribosomal proteins (NES = −3.21 to −3.41, FDR < 0.001). These patterns suggest higher basal protein synthesis capacity in females.

GSEA of sex comparisons revealed strong enrichment for ribosomal components among female-biased genes, including ribosome (KEGG; NES = −3.20 to −3.35, FDR < 0.001), cytoplasmic ribosomal proteins (WikiPathways; NES = −3.21 to −3.41, FDR < 0.001), and peptide biosynthetic process (GO:0043043; NES = −3.22, FDR < 0.001). These sex-biased patterns were largely conserved across drug conditions, with 104 male-biased and 79 female-biased pathways shared between CFA and CNR-401 contexts (Supplementary Table S7).

Convergent and divergent pathway themes

Cross-comparison analysis identified both shared and compound-specific pathway signatures (Figure 9; Supplementary Table S6). Of the 858 CFA-significant and 434 CNR-401 -significant pathways, 255 were shared between compounds, including 20 concordantly upregulated and 70 concordantly downregulated pathways.

Convergent themes included: (i) suppression of mucin-type O-glycan biosynthesis (CFA NES = −2.40, CNR-401 NES = −2.45, FDR < 0.001) and O-glycan processing; (ii) downregulation of lysosomal function (CFA NES = −2.33, CNR-401 NES = −1.72) and retinoid metabolism (CFA NES = −2.05, CNR-401 NES = −2.42); (iii) shared upregulation of G-protein-coupled receptor signaling, including heterotrimeric G-protein complex (CFA NES = 2.06, CNR-401 NES = 2.31, FDR < 0.001) and adenylate cyclase-modulating GPCR signaling (CFA NES = 2.08, CNR-401 NES = 2.34, FDR < 0.001); and (iv) upregulation of ribonucleoprotein complex biogenesis (CFA NES = 1.82, CNR-401 NES = 2.13, FDR < 0.05).

Divergent themes were revealed by drug comparison analysis (726 significant pathways). Relative to CFA, CNR-401-treated samples showed enrichment for ribosome biogenesis (NES = 2.67, FDR < 0.001), rRNA processing (NES = 2.65, FDR < 0.001), and branched-chain amino acid degradation (NES = 2.60, FDR < 0.001). Conversely, CFA treatment showed relative enrichment for glutamatergic synaptic signaling (CNR-401 versus CFA: NES = −2.70, FDR < 0.001), postsynaptic density components (NES = −2.78, FDR < 0.001), and ionotropic glutamate receptor complex (NES = −2.78, FDR < 0.001), indicating that synaptic function pathways are preferentially activated by CFA.

Sex-biased pathways showed remarkable conservation across drug conditions. Conserved male-biased pathways included glucuronidation (CFA NES = 2.65, CNR-401 NES = 2.58), triglyceride metabolism (CFA NES = 2.12, CNR-401 NES = 2.16), and transport of inorganic cations/anions and amino acids (CFA NES = 1.98, CNR-401 NES = 2.75). Conserved female-biased pathways included ribosome (CFA NES = −3.35, CNR-401 NES = −3.20), cytoplasmic ribosomal proteins (CFA NES = −3.41, CNR-401 NES = −3.21), and selenoamino acid metabolism (CFA NES = −3.44, CNR-401 NES = −3.09). This conservation of sex-biased pathway signatures regardless of drug treatment indicates robust sexual dimorphism in baseline metabolic and biosynthetic programs.

Figure 9. Shared enriched pathways between CFA and CNR-401 treatment responses

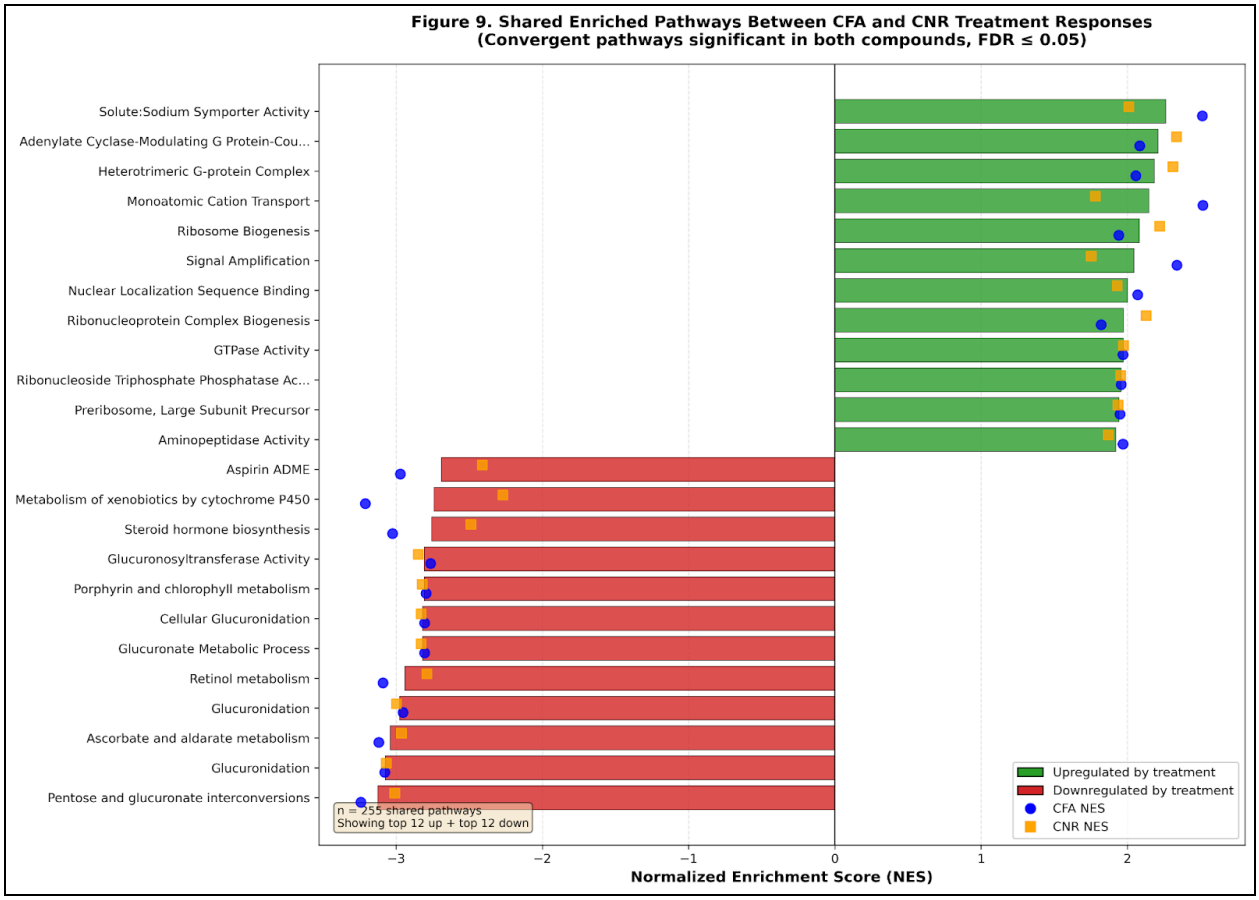

Horizontal bar plot showing GSEA pathways significantly enriched in both CFA and CNR-401 treatment comparisons (FDR ≤ 0.05 in both). Bars represent average normalized enrichment score (NES) across compounds; individual CFA (blue circles) and CNR-401 (orange squares) NES values shown. Green bars indicate pathways upregulated by treatment; red bars indicate pathways downregulated. Convergent upregulated pathways include G-protein-coupled receptor signaling (adenylate cyclase-modulating GPCR, heterotrimeric G-protein complex), ribosome biogenesis, and GTPase activity. Convergent downregulated pathways include glucuronidation, pentose and glucuronate interconversions, xenobiotic metabolism by cytochrome P450, retinol metabolism, and steroid hormone biosynthesis. Of 858 CFA-significant and 434 CNR-401 -significant pathways, 255 were shared between compounds (90 with concordant direction: 20

upregulated, 70 downregulated). GSEA performed with gseapy using 1,000 permutations; genes ranked by Wald statistic.

Protein-protein interaction network analysis

To identify potential regulatory hubs, differentially expressed genes (DEGs, FDR < 0.05) from each contrast were queried against the STRING protein-protein interaction database (v11.5, *Drosophila melanogaster*, interaction score ≥ 0.4). Network statistics and hub genes (defined as the top 10 genes by degree centrality within each network) are summarized in Table 6 and Supplementary Table S8.

Sex-dimorphic networks.

Among networks with ≥50 nodes, the CNR-401 treated male versus female comparison yielded the largest interaction network (100 nodes, 564 edges, clustering coefficient 0.39), with the main connected component encompassing 57% of nodes (Fig. 9A). In contrast, the corresponding CFA sex comparison (102 nodes, 153 edges, clustering coefficient 0.25) exhibited more sparse connectivity, with its largest component containing only 28% of nodes. Notably, 57 of the top 100 hub genes across all sex-comparison networks are shared between CFA and CNR-401 treatments (Jaccard index 0.51), with recurrent hub genes appearing in multiple networks (Supplementary Table S8). STRING functional enrichment analysis of these recurrent hubs revealed significant enrichment for olfactory transduction (FDR < 10^{-8}), sensory perception (FDR < 10^{-7}), and ionotropic glutamate receptor signaling (FDR < 10^{-4})

Treatment-effect networks.

For treatment contrasts (treated versus control), the CFA male treatment comparison (36 nodes, 76 edges, clustering coefficient 0.40) formed a cohesive network with 94% of nodes in a single

connected component (Fig. 9B), enriched for one-carbon metabolism (FDR = 2.3×10^{-4}) and folate biosynthesis (FDR = 3.1×10^{-3}). Hub genes included folate-cycle enzymes (Shmt, AdSL, Nmdmc) and heat-shock proteins (Hsp26, Hsp27, Hsp70Bb). The sex-adjusted treatment contrasts (fewer DEGs by design) produced smaller networks: CFA (14 nodes, 12 edges) and CNR-401 (5 nodes, 3 edges). Density values for these small networks are omitted from cross-contrast comparisons, as network density is inherently inflated when node counts are low ($N < 30$).

Recurrent hub genes.

Across all pairwise contrasts, 95 genes were identified as hubs in three or more networks (Supplementary Table S8). The most frequently recurring hubs—Ir8a, Or56a, Or92a, and Obp83a (each present in 6 networks)—encode olfactory and odorant-binding receptors, suggesting that chemosensory pathways may be a conserved transcriptional target across treatment and sex conditions.

Table 6. STRING network statistics for selected DEG contrasts.

DEGs, differentially expressed genes (FDR < 0.05); CC, connected component. Density and clustering omitted for networks with <30 nodes. Full network statistics in Supplementary Table S9.

Comparison	DEGs (N)	Nodes	Edges	Density	Clustering	Largest CC (%)

CNR-401 treated male vs female	179	100	564	0.114	0.393	57 (57%)
CNR-401 control male vs female	205	108	280	0.048	0.368	76 (70%)
CFA control male vs female	219	102	153	0.030	0.246	29 (28%)
CFA male treated vs control	40	36	76	0.121	0.402	34 (94%)
CFA treated vs control (adj sex)	27	14	12	—	—	4 (29%)
CNR-401 treated vs control (adj sex)	6	5	3	—	—	3 (60%)

Weighted gene co-expression network analysis

A total of 4,989 genes (mean count ≥ 10 across samples) were clustered into 10 co-expression modules plus a residual "grey" module containing 1,463 unassigned genes (29.3%; Table 7). Module eigengenes were correlated with sample traits (drug, sex, treatment), and hub genes were identified as the top 20 genes per module ranked by the product of module membership (MM) and intramodular connectivity (kME).

Sex-associated modules

Two large modules exhibited strong sex associations: Module 9 (1,142 genes; r = −0.95 with female, FDR < 10^{-15}) and Module 2 (1,079 genes; r = +0.94 with male, FDR < 10^{-14}). Module 9 hub genes encode ribosomal subunits (RpS10b, RpL18A, mRpL16), suggesting female-biased ribosome biogenesis. Module 2 hub genes include chemosensory receptors (Obp83a, Or56a, Ir8a), consistent with male-biased olfactory gene expression. A third module, Module 4 (222 genes; r = +0.71 with male, FDR < 10^{-5}), is enriched for mitochondrial complex I components (ND-75, ND-42, ND-30; Supplementary Table S11).

Drug-associated modules

Module 10 (214 genes) showed the strongest drug association (r = −0.94, indicating CFA-biased expression; FDR < 10^{-14}). Hub genes include ionotropic receptors (Ir75b, Ir75c, Ir64a), which function in gustatory and olfactory perception. Module 3 (122 genes; r = −0.78 with CFA, FDR < 10^{-6}) hub genes encode detoxification enzymes (Ugt86Dd, Cyp6g1, Cyp6g2), suggesting drug-specific induction of xenobiotic metabolism.

Treatment-associated module

Only Module 8 (102 genes) showed significant correlation with treatment status (r = −0.55, FDR = 0.005), indicating reduced expression in treated versus control samples across both drugs. Hub genes include lipid desaturase (Desat1), endoplasmic reticulum chaperone (Hsc70-3), and JNK pathway component (Src64B; Supplementary Table S11).

Module-DEG overlap

To assess concordance between WGCNA and pairwise DEG analyses, we computed the fraction of each module's genes present in each DEG set. Module 10 showed 38% overlap with CFA

male treated versus control DEGs (hypergeometric $p < 10^{-8}$), and Module 8 showed 22% overlap with the same contrast ($p < 0.01$). Module 9 and Module 2 showed > 40% overlap with all four sex-comparison DEG sets, confirming that sex-driven expression signatures are robust across both drugs (Supplementary Table 10; Supplementary Fig. S7).

Table 7. WGCNA module summary.

r, Pearson correlation between module eigengene and trait; FDR, Benjamini-Hochberg adjusted p-value. Only the top-associated trait per module is shown; full correlations in Supplementary Table S10

NS, not significant. An additional 1,463 genes (29.3%) were not assigned to any module.

Module	Genes	Top Trait	r	FDR	Top Hub Genes
Module 9	1,142	Sex (F)	−0.95	$<10^{-15}$	RpS10b, RpL18A, mRpL16
Module 2	1,079	Sex (M)	+0.94	$<10^{-14}$	Obp83a, Or56a, Ir8a
Module 10	214	Drug (CFA)	−0.94	$<10^{-14}$	Ir75b, Ir75c, Ir64a
Module 4	222	Sex (M)	+0.71	$<10^{-5}$	ND-75, ND-42, ND-30

Module 3	122	Drug (CFA)	−0.78	$<10^{-6}$	Ugt86Dd, Cyp6g1, Cyp6g2
Module 8	102	Treatment	−0.55	0.005	Desat1, Hsc70-3, Src64B
Module 6	297	Sex (F)	−0.55	0.005	sug, GstE1, CG7214
Module 1	76	Sex (M)	+0.73	$<10^{-5}$	Cyp309a1, mmy, sro
Module 5	238	—	NS	—	—
Module 7	34	Sex (F)	−0.41	0.050	CG14545, CG10513

Figure 10. Module-trait correlation heatmap from weighted gene co-expression network analysis.

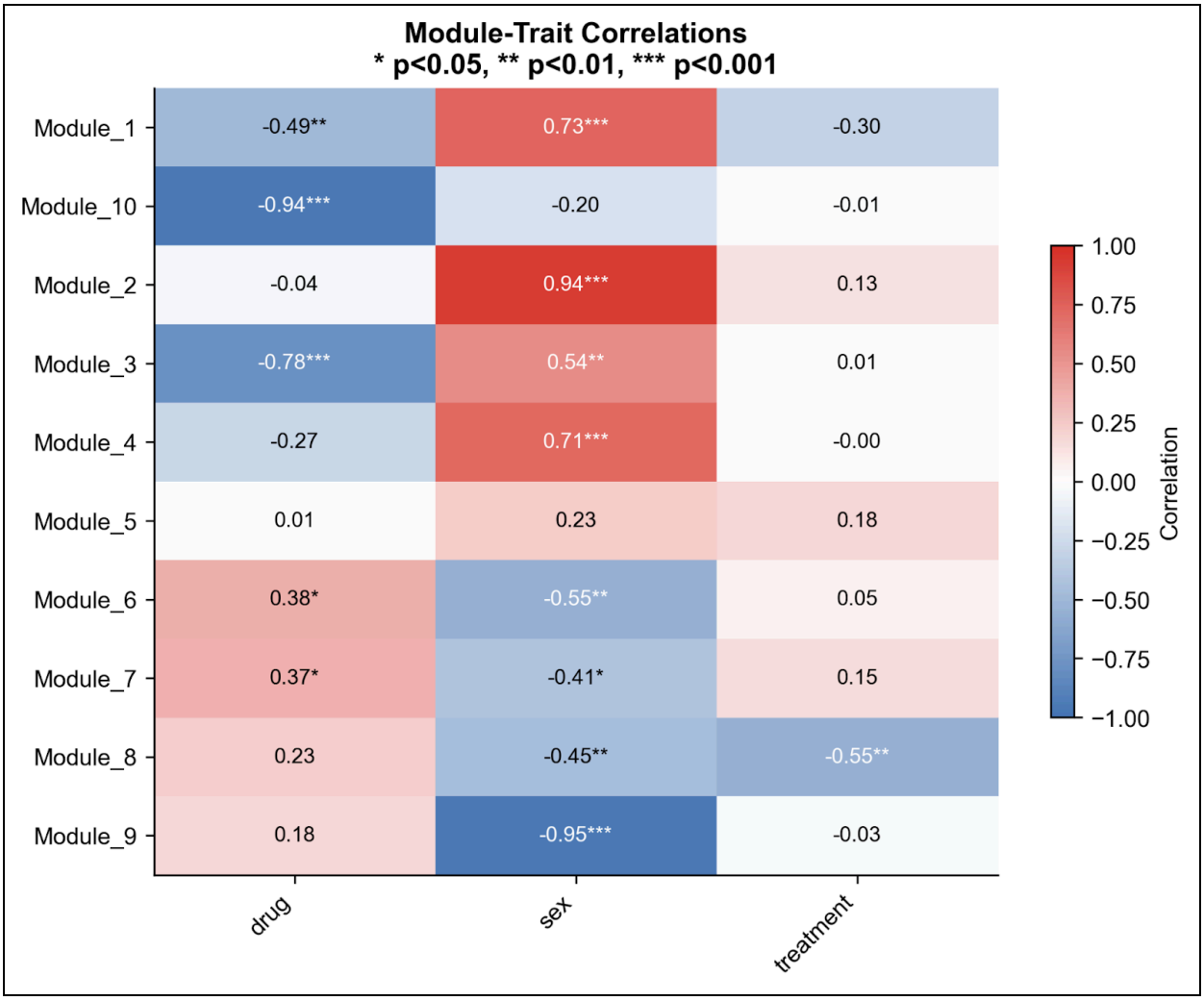

618

619 *Heatmap displaying Pearson correlation coefficients between module eigengenes (rows) and*
620 *experimental traits (columns). Color scale indicates correlation direction and magnitude (blue =*
621 *negative, red = positive). Asterisks denote statistical significance (* $p < 0.05$, ** $p < 0.01$, *** p*
622 *< 0.001; Benjamini-Hochberg corrected). Module 10 shows strong CFA-associated expression (r*
623 *$= -0.94$ with drug). Module 9 ($r = -0.95$) and Module 2 ($r = +0.94$) represent robust female-*
624 *and male-biased modules, respectively. Module 8 is the only module significantly correlated with*
625 *treatment status ($r = -0.55$), indicating downregulation in treated samples. Module 3 shows dual*
626 *associations with drug ($r = -0.78$, CFA-biased) and sex ($r = +0.54$, male-biased).*

Discussion

The transcriptional states produced by Cannflavin A and CNR-401 map onto established pathological axes of Amyotrophic Lateral Sclerosis (ALS), Frontotemporal Dementia (FTD), Parkinson's Disease (PD), and Alzheimer's Disease (AD). This explains the mechanisms through which these drugs exhibit neuroprotective effects, such as rescuing motor phenotypes in zebrafish impaired with the neurotoxin β-N-methylamino-L-alanine (BMAA) (Banwait et al., 2025).

Coordinated Suppression of Drug Metabolism

GSEA revealed glucuronidation-related processes among the most strongly downregulated pathways in both treatments (Table 4), appearing consistently across all four databases. Glucuronidation is a phase II detoxification pathway (Josephy et al., 2005) in which UDP-glucuronosyltransferases (UGTs) attach a water-soluble group to lipophilic compounds, conjugating them into hydrophilic glucuronides and facilitating their excretion by phase III ABC transporters (Yan et al., 2025; Yang et al., 2017). Treatment with CFA and CNR-401 impaired not only the conjugation process but also the upstream metabolism of sugars to create the water-soluble group (see Pentose and glucuronate interconversions in Supplementary Table S6), indicating a coordinated systemic suppression.

Increasing Drug Bioavailability

This suppression may aid in the bioavailability of the drugs, prolonging their therapeutic effects. The metabolism of drugs in the brain is handled by either one or both of phase I functionalization by cytochrome P450s (CYPs) and/or phase II glucuronidation by UGTs before final phase III export by ABC transporters (Josephy et al., 2005; Yan et al., 2025; M. Zhang et al., 2024). For

luteolin, the chemical precursor of cannflavins (Abdel-Kader et al., 2023; Rea et al., 2019), glucuronidation is the primary elimination pathway (Yang et al., 2017). This is generally the case for the aglycone forms of polyphenols (Hu, 2007). While cannflavins, cannabinoids, and terpenes are functionally aglycones, in that they lack a sugar group, only cannflavins possess the multiple phenolic rings required to be classified as polyphenols (Abdel-Kader et al., 2023; Rea et al., 2019). Whether or not glucuronidation is the primary pathway for the specific ingredients in CNR-401 requires further investigation. However, since CFA and CNR-401 also downregulate the metabolism of xenobiotics by cytochrome P450s (Supplementary Table S6), it can be conservatively inferred that these drugs downregulate the pathways that would otherwise inactivate and clear them, extending the duration of their effects. This would be a powerful property given that common dietary polyphenols are known to have poor bioavailability, typically 2-20% (Hu, 2007), which is most attributed to their rapid glucuronidation once ingested (Gao & Hu, 2010; Hu, 2007). In the past, the bioavailability of the polyphenol curcumin has been increased by 2000% in humans when administered with piperine (Shoba et al., 1998), a known inhibitor of glucuronidation (Lambert et al., 2004; Shoba et al., 1998).

Supporting the Endogenous Neuroprotection of Steroids

Another interpretation is that by suppressing glucuronidation, CFA and CNR-401 are extending the lifespan of endogenous neuroactive compounds. Phase I-III detoxification genes are highly expressed in the brain where they function to regulate the elimination of neurosteroids and neurotransmitters (Sheng et al., 2021; Silva-Adaya et al., 2021; Yan et al., 2025). Neurosteroids have extensively been shown to protect against neurodegeneration (Borowicz et al., 2011; Garcia-Segura & Balthazart, 2009; Puig-Bosch et al., 2023). Estrogen-like steroids are particularly powerful (Brann et al., 2007; Bustamante-Barrientos et al., 2021), having been

shown to exert an anti-apoptic effect on spinal motor neurons in rats (Cardona-Rossinyol et al., 2013; Chen et al., 2015). This is of particular significance considering that motor neuron death is the central characteristic of ALS pathophysiology (Hardiman et al., 2017).

Complex Effects on other Compounds in the Brain

The effects of suppressed glucuronidation on other substrates in the brain, such as dopamine and cholesterol (Silva-Adaya et al., 2021; Yan et al., 2025) remains unclear. Increasing the lifespan of dopamine in the brain is of relevance to PD, where pathological symptoms are attributed to decreased dopamine in the substantia nigra (Zhou et al., 2023). While inhibition of CYP2E1 has previously been shown to increase extracellular dopamine concentration in the substantia nigra of rats (Nissbrandt et al., 2001), CYP2D can synthesize dopamine from tyramine (Sheng et al., 2021) showing that the CYPs are a diverse family with contradicting effects between different members. This homeostatic interplay is also present for cholesterol, where brain CYPs are involved in both its biosynthesis and catabolism (Sheng et al., 2021). While it is important to know how CNR-401 and CFA affect specific members of these families, for example *CYP2E1* and *CYP2D*, gene-level statements cannot be made because their orthologs do not exist or are not yet annotated in the *Drosophila* genome (Drosophila_melanogaster - Ensembl Genome Browser 113, 2024). Additionally, the metabolism of compounds in the brain is not limited to just CYPs and UGTs. Using dopamine as an example, it is primarily eliminated by aldehyde dehydrogenase and catechol methyltransferase, with UGTs and sulfotransferases providing alternative routes (Sheng et al., 2021). Thus, it is important to assess the transcriptomic impact on other detoxification processes to gain a more holistic view of how the metabolism of neuroactive compounds are modulated.

Divergent Regulation of Other Detoxification Pathways

While both CFA and CNR-401 show negative enrichment of UGT and CYP metabolic pathways, they have divergent effects on other detoxification pathways. CNR-401 maintains or upregulates other phase II processes (Yan et al., 2025) including glutathione metabolism (NES = 1.880) and sulfotransferase activity (NES = 1.971), while CFA downregulates these same processes (NES = -1.984 and -1.862). This appears to be evidence of induction of a metabolic switch rather than a complete shutdown of detoxification: endogenous compounds in the brain exhibit the metabolic flexibility to use multiple detoxification pathways (Sheng et al., 2021; see discussion of dopamine above) evidenced by the fact that phase II enzymes share substrates (Ouzzine et al., 2014). By targeting specifically UGTs and CYPs, CNR-401 slows metabolism, but does not halt it systemically like CFA does, preventing toxic accumulation and overload. The same up/down pattern is also present in the regulation of phase III ABC transporters (CNR-401 NES = 3.17. CFA NES = -2.88; Supplementary Table S6), where CNR-401 uniquely maintains the "revolving door" that allows the compounds to actually leave the cell once metabolized (Liu & Hu, 2007). This theory of superior modulation of detoxification is supported by the fact that CNR-401 was shown to be less toxic than CFA in zebrafish embryos: 62.5% versus 37.5% larval survival at 5 µM (Banwait et al., 2025).

Glutathione as an Antioxidant

Glutathione is not only a phase II detoxification enzyme, but also a major antioxidant in the brain (Aoyama, 2021; Silva-Adaya et al., 2021). Decreased expression in the glutathione S-transferases (GSTs) responsible for attaching glutathione to compounds, namely *GST01* and *GST02*, have been associated with an earlier age of onset for AD, fALS, and PD (Kölsch et al.,

2004; Li et al., 2003; Van De Giessen et al., 2008). Additionally, increased *GSTP1* expression reduces hyperactive cyclin dependent kinase-5 (Cdk5) activity by direct competitive inhibition and neutralizing oxidative stress, preventing it from driving AD through Aβ production and PD through degeneration of dopaminergic neurons in the substantia nigra (Allnutt et al., 2020; Sun et al., 2011). The upregulation of glutathione metabolism by CNR-401 thus suggests a powerful antioxidant mechanism of action.

ABC Transporters as Regulators of Inflammation and Neurodegeneration

The upregulation of ABC-transporter genes is also meaningful. These ATP-dependent transporters protect the central nervous system (CNS) by acting as a barrier against toxic substances (Yan et al., 2025) as well as by governing the homeostasis of lipids (Kotlyarov & Kotlyarova, 2021). ABCB1 and ABCG2 control the delivery of drugs into the brain at the blood brain barrier (Schulz et al., 2023), and their increased expression suggests better protection against neurotoxins (Schulz et al., 2023; Yan et al., 2025). Within the brain, the engagement of lipid-trafficking is consistent with neurodegeneration frameworks that place lipid-homeostasis and transporter-linked expression at the interface of cholesterol handling and inflammation (Villa et al., 2024). Specifically, the observed upregulation of *ABCG2* (L2FC = 0.24 and 0.29, FDR = 0.02 and 0.002; see FBgn0052091 and FBgn0031449 in Supplementary Table S5) aligns with the relief of oxidative stress and neuroinflammation in brain tissue (Shen et al., 2010). The role of *ABCA1* can be highlighted as a candidate gene for Alzheimer's disease (Fehér et al., 2018; Yan et al., 2025) where mice models have shown that lack of ABCA1 increases amyloid-β deposition and cognitive decline while overexpression of *ABCA1* decreases amyloid-β plaques (Koldamova et al., 2014). CNR-401's ability to upregulate this gene (L2FC = 0.33, FDR = 0.05; see FBgn0034493 in Supplementary Table S5) aligns with these neuroprotective mechanisms,

suggesting its potential as a therapeutic treatment for AD. There is also potential application to PD, since the decrease or loss-of-function in genes including *ABCA7*, *ABCB7*, *ABCA5*, and *ABCB1* have all been associated with disease development (Yan et al., 2025). Conservatively, the transcriptomic impact of CNR-401 can be said to move the system toward a neuroprotective state by controlling lipid-based inflammation and toxin vulnerability, relevant to neurodegeneration.

CNR-401 Uniquely Affects Lipid Trafficking and Metabolism

When looking at the most significant pathways affected differently between treatments (Supplementary Table S6), lipid metabolism pathways consistently emerge as being uniquely upregulated by CNR-401. It is important to note here that the excipient used to deliver the compounds contained a heavy concentration of long-chain fatty acids. However, this same excipient was also used to deliver CFA and results from this experiment showed an opposite negative regulation (Supplementary Table S6), indicating that the observed effects on lipid metabolism cannot be attributed solely to the excipient. The source of the following observed effects should be verified by repeating the experiment(s) with the excipient added to the control group. Nonetheless, this excipient is part of the final formulation; so, it is part of CNR-401 and can be discussed as such.

Strong positive enrichment was observed for very-long-chain, long-chain, unsaturated, and regular fatty acid metabolism (NES = 2.732, 2.882, 2.353, 2.771), as well as for gene sets involving fatty acid transport, oxidation, biosynthesis, elongation, degradation, and catabolism (Supplementary Table S6). This suggests that CNR-401 drives a widespread lipid-metabolic response in neural tissue, mechanistically relevant to ALS since metabolic alterations are including hypermetabolism and altered energy expenditure are well-documented, and lipid

profile changes vary with disease phase and clinical phenotype (Burg & Van Den Bosch, 2025; Dorst et al., 2023; Maruyama et al., 2023; Nakamura et al., 2021). There is also a connection to AD, since cholesterol is known to increase the production and deposition of Aβ peptides, leading to the formation of amyloid plaques (Sheng et al., 2021).

CNR-401 treatment also uniquely resulted in positive enrichment of peroxisome-related pathways (NES ≃ 2; Supplementary Table S6). Peroxisomes lie at the intersection of very-long-chain fatty-acid metabolism and ether-lipid biology and participate in redox-linked lipid homeostasis processes (Wanders & Waterham, 2006). These findings strengthen the role of the upregulated ABC transporters (discussed above) in lipid trafficking. Of the 48 ABC transporters, 20 are thought to transport lipids or lipid-related compounds (Tarling et al., 2013), with ABCD1, ABCD2 and ABCD3 bound to the peroxisomal membrane where they transport fatty acids into the peroxisome for oxidation (Kemp et al., 2011). Taken together, the coordinated induction of lipid metabolism, peroxisomal, and ABC transporter pathways provides a link between lipid turnover and organelle-based processing. These results indicate that CNR-401 shifts the transcriptome toward a lipid-metabolic state corresponding to major pathology axes inn neurodegenerative diseases.

CFA Uniquely Affects Synaptic Activity and Energy Production

Glutamate Excitotoxicity and ALS

Enrichment analysis of CFA treatment effects reveals a robust upregulation of gene sets associated with synaptic function and the regulation of neuronal excitability; the top 100 upregulated pathways are overwhelmingly dominated by these terms (Supplementary Table S6). This is of extreme relevance to ALS, where the two most long-standing FDA approved drugs,

edaravone and riluzole, target excitotoxicity in neurons (Arnold et al., 2024; Hardiman et al., 2017). In the "cortical hyperexcitability hypothesis" of ALS (Arnold et al., 2024), excessive glutamate signalling, though the activation of postsynaptic ionotropic receptors, causes repeated firing of motor neurons eventually becoming toxic and leading to cell death (Dong et al., 2009; Hardiman et al., 2017). This is believed to preferentially affect motor neurons because of their relatively low ability to buffer intracellular calcium ions (Ca^{2+}), leading to mitochondrial overload and initiation of apoptosis (Dong et al., 2009; Hardiman et al., 2017; Van Den Bosch et al., 2006).

Modulation at the Synapse

The primary processes that cause excitotoxicity at the synapse (Arnold et al., 2024) were significantly affected by CFA treatment. Most notably, upregulation was found for Glutamatergic Synaptic Transmission (NES = 3.165), Ionotropic Glutamate Receptor Complex (NES = 2.783), and Glutamate Binding and Activation of AMPA Receptors (NES = 2.175; all results for this section in Supplementary Table S6). While this is immediately associated with an excitotoxic state (Arnold et al., 2024), this excitatory response was crucially balanced by a simultaneous induction of inhibitory signalling. CFA treatment upregulated GABAergic Synapse (NES = 2.175) which is meaningful given that decreased inhibitory currents and reduced GABAergic synapse densities are observed in mice models of ALS (W. Zhang et al., 2016). Additionally, CFA promotes neuron health through upregulation of the Synaptic Vesicle Cycle pathway (NES = 2.731), which is impaired by hyperexcitability-associated (Weskamp et al., 2020) TDP43 alterations in ~97% of ALS patients (Hardiman et al., 2017).

These balanced synaptic adjustments align with homeostatic plasticity principles, where neural circuits adjust excitatory and inhibitory conductances to maintain stable output during perturbations (O'Leary et al., 2014; Turrigiano, 2012). For example, elevated intracellular Ca^{2+} though voltage-gated channels activated by chronic potassium ion (K^+) depolarization can actually prevent apoptosis (Ichinose et al., 2003). This mechanism-of-action is strongly supported though CFA's strong upregulation of Potassium Channel Activity (NES = 3.165), Potassium Ion Transport (NES = 2.866), Leak Channel Activity (NES = 2.759), Calcium Ion Transmembrane Transport (NES = 2.049), Regulation of Cytosolic Calcium Ion Concentration (Nes = 1.869), and Regulation of Voltage-Gated Calcium Channel Activity (NES = 2.076). This suite of pathways is importantly coupled with Potassium Ion Homeostasis (NES = 2.832), Calcium Ion Homeostasis (NES = 1.874), and Stabilization of Resting Membrane Potential (NES = 2.789). These findings also align with clinical observations that pharmacologically activating the Kv7 family of K^+ channels successfully decreases motor neuron excitability in ALS patients (Wainger et al., 2014, 2021), altogether suggesting that modulating potassium conductance is a viable strategy for stabilizing neurons against excitotoxicity,

Downstream Regulation of Calcium-Buffering Organelles

Excitotoxicity is also defined by secondary processes: the response of calcium-buffering organelles such as the endoplasmic reticulum (ER) and mitochondria (Arnold et al., 2024). Changes to mitochondrial morphology and function are well-documented in ALS (Onesto et al., 2016; Salvatori et al., 2018; P. Wang et al., 2019; W. Wang et al., 2016), where they are associated with disrupted respiratory chain function and production of reactive oxygen species (ROS) (Hardiman et al., 2017; Taylor et al., 2016). Specifically, the poly(GR) dipeptide repeat in *C9ORF72*-ALS has been shown to bind to mitochondria and cause dysfunction (Choi et al.,

2019; Dafinca et al., 2016; Lopez-Gonzalez et al., 2016). Considering this knowledge, the upregulation of Oxidative Phosphorylation (NES = 1.922) by CFA signals healthy mitochondrial function and a shift away from calcium-overload and ALS pathophysiology. In 5-20% of mitochondria, excess calcium is shared with the ER through mitochondria-associated ER membranes, with calcium-overload in the ER causing the unfolded protein response (UPR) (Arnold et al., 2024; Bhardwaj et al., 2019), also associated with ALS onset (Pharaoh et al., 2019). Response to Unfolded Protein and the Mitochondrial Outer Membrane were notably downregulated (NES = -2.211 and -1.647 in Supplementary Table S6), however orthologs of ER-mitochondria tethering proteins (FBgn0029687and FBgn0029999 in Supplementary Table S5) were not found to be significantly affected in either direction. To further clarify the effect on ER stress and the UPR, it would be helpful to make comparisons to a healthy control. For the scope of this study, it can be said that CFA induces a robust effect on synaptic pathways directly related to the excitotoxic pathophysiology of neurodegenerative diseases,with therapeutic potential through principles of homeostatic plasticity.

Energy Production and ALS

Fatigue is a common symptom for ALS patients, thought to be caused by ATP depletion in motor neurons (Alencar et al., 2022; Vandoorne et al., 2018). As previously mentioned, CFA induced a significant upregulation of Oxidative Phosphorylation (NES = 1.922), suggesting engagement of metabolic machinery to support neuronal energy demands. CNR-401 showed an opposite downregulation of Oxidative Phosphorylation (NES =1.665), but an upregulation of Mitochondrial Fatty Acid Beta-Oxidation (NES - 1.777). Coupled with the robust lipid metabolic signature previously explored, this suggests that CNR-401 enacts a metabolic switch from

glucose to fatty acids (Veech, 2004). This is an established therapeutic shift that is known to increase ATP output and decrease the production of free radicals (Seyfried et al., 2019; Veech, 2004), and is emerging as a promising treatment for ALS patients (Phillips et al., 2024). These contrasting signatures support a model where the drugs engage distinct mitochondrial pathways, but converge on a mechanism of increased energy production. This may help neuronal survival, and at the very least increase patient quality-of-life. The ability of CNR-401 to engage ketogenic metabolism is especially interesting and warrants further investigation.

Circadian and Stress-Linked Pathways

Both CFA and CNR-401 produced consistent transcriptional modulation of the core circadian clock, with particularly strong suppression of the negative arm of the molecular oscillator. In both treatments, timeless (tim) was among the most strongly downregulated genes (CFA LFC = −1.17; CNR-401 LFC = −1.13), and period (per) was similarly reduced (CFA LFC = −0.78; CNR-401 LFC = −0.82). In contrast, the positive arm component clock (clk) showed modest but significant upregulation (CFA LFC = +0.41; CNR-401 LFC = +0.34), while cryptochrome (cry) and doubletime (dbt) remained largely unchanged. Together, this pattern suggests a coordinated damping of the PER–TIM negative feedback loop accompanied by relative enhancement of CLK driven transcriptional output (Allada et al., 2001).

Circadian disruption is increasingly recognized as a contributing factor in ALS and ALS/FTD, with patients exhibiting altered sleep–wake cycles (Lang, 2025). The coordinated modulation of tim, per, and clk observed here indicates that both compounds engage clock-linked stress and metabolic pathways with potential relevance to ALS pathogenesis. Importantly, the circadian clock is tightly integrated with lipid metabolism and inflammatory signaling (Bass & Takahashi,

2010; Gerstner et al., 2023; Konakchieva et al., 2025; Milling, 2020; Petrenko et al., 2023; X. Wang et al., 2020), providing a mechanistic bridge between the circadian signatures observed here and the lipid centric effects especially prominent in the CNR-401 transcriptomic response discussed previously. In mammalian astrocytes, a type of glial cell, the core clock component BMAL1 (the mammalian CLK partner) regulates autophagy, endolysosomal flux, and lipid remodeling, and its loss leads to profound defects in lysosomal function and neuroinflammation (McKee et al., 2023). These pathways align directly with the CNR-401-dependent upregulation of fatty acid metabolism and peroxisomal remodeling, suggesting that the drug's lipid metabolic phenotype may in part arise from clock-linked regulation of glial lipid handling.

Taken together, the transcriptomic data indicate that CFA and CNR-401 converge on a shared core circadian mechanism, suppression of PER/TIM and enhancement of CLK, with CNR-401 coupling them to lipid metabolic, peroxisomal, and transporter mediated pathways. This supports a model in which cannabinoid derived interventions engage clock-linked nodes controlling lipid metabolism, autophagy, and stress resilience, all of which are central to ALS/FTD vulnerability.

Conclusions

In a C9orf72 *Drosophila* model of ALS/FTD, treatment with CFA and CNR-401 exhibits transcriptomic responses relevant to Amyotrophic Lateral Sclerosis (ALS), Frontotemporal Dementia (FTD), Parkinson's Disease (PD), and Alzheimer's Disease (AD). Strong downregulation of detoxification pathways suggest increased drug bioavailability (Gao & Hu, 2010; Yan et al., 2025; Yang et al., 2017) and support of endogenous neuroprotective steroids (Borowicz et al., 2011; Garcia-Segura & Balthazart, 2009; Puig-Bosch et al., 2023), with CFA causing a systemic suppression and CNR-401 eliciting a more targeted inhibition of

glucuronidation while enhancing other detoxification mechanisms such as export by ABC transporters and conjugation by glutathione. The strong upregulation of ABC transporters and lipid metabolism shown uniquely by CNR-401 indicates modulation of inflammation (Shen et al., 2010; Villa et al., 2024) and aligns with therapeutic potential for neurodegenerative diseases (Yan et al., 2025). Furthermore, the metabolic shift to mitochondrial fatty acid oxidation hints at a ketogenic mechanism (Veech, 2004), relevant to the fatigue common in ALS patients (Alencar et al., 2022). CFA was shown to induce a distinct response characterized by broad synaptic remodeling and regulation of excitotoxicity (Arnold et al., 2024; Dong et al., 2009), as well as support of mitochondrial oxidative phosphorylation. These findings suggest that CFA and CNR-401 produce distinct but potentially complementary transcriptional states that align with pathways implicated in neurodegenerative diseases. While CNR-401 focuses on managing lipid metabolism and neuroinflammation with the engagement of glutathione to scavenge free radicals, CFA targets synaptic homeostasis by controlling calcium overload and excitotoxicity.

In order to further explore the mechanisms of action of these two drugs, future studies should utilize mammalian models of ALS to facilitate better ortholog mapping and support gene-level claims. This would aid in the understanding of the impact on complex gene families where members have divergent or interactive effects. Interpretation would also benefit from the inclusion of a healthy control group in addition to a pathological control, with the excipient added to all groups. It would also be interesting to investigate the isolated effects of other CNR-401 ingredients, given the distinct signature of CFA. For now, the mechanisms of action for these two treatments have been shown to be relevant to neurodegenerative pathophysiology.

Coupled with toxicity assays and phenotypic evidence (Banwait et al., 2025), CNR-401 is a strong therapeutic candidate for ALS patients.

Data and Code Availability

Supplementary materials are available in this public repository: https://figshare.com/projects/Transcriptomic_Effects_of_Cannabis-Derived_Therapies_in_a_Drosophila_model_of_ALS/271489

Figure S1. Sample QC summary

Figure S2. Normalization Size factors

Figure S3. Sample Count distributions

Figure S4. Sample Correlation PCA Plots

Figure S5. Sample Correlation Heatmaps

Figure S6. LFC distributions

Figure S7. WGCNA Module-DEG overlap

Table S1. RNA Extraction Stats

Table S2. RNA Sequencing Stats

Table S3. Counts matrix

Table S4. Sample QC Metrics

Table S5. DEA Results

Table S6. Treatment Effect GSEA Pathways

Table S7. Sex Effect GSEA Pathways

Table S8. STRING Recurrent Hub Genes

Table S9. STRING Network Statistics

Table S10. WGCNA Module-Trait Correlations

Table S11. WGCNA Hub Genes

Code used in this study can be found in this public repository:
https://github.com/gdeol4/drosophila-deseq2-workflow

Acknowledgements

The authors thank Theresa Niccoli at University College London, Institute of Healthy Ageing for providing the *UAS-C9orf72*$_{polyGR36}$ males used in this study.

The authors thank David Konkin at NRC Canada for performing the RNA extraction and sequencing, as well as processing the raw reads.

The authors thank Ethan B. Russo, MD of CReDO Science and Senior Medical Advisor at Canurta for assisting with the interpretation of the upregulation of ABC-transporter genes.

Author Contributions

G.D. and I.B. analyzed the data and wrote the manuscript.

S.C., and T.T.D. performed the experiments.

T.T.D., J.G., K.B., E.S., and J.A.C. designed the experiments and reviewed the manuscript.

A.G. coordinated and supported the entire research effort.

All authors read and approved the final manuscript.

Conflicts of Interest

Authors G.D., I.B., K.B., E.S., J.A.C., and A.G. are employed by Canurta Therapeutics, which funded the research.

Ethical Approval

Ethical approval was not required for these invertebrate experiments.

Consent to Participate

Consent was not required for the performed study.

References

Abdel-Kader, M. S., Radwan, M. M., Metwaly, A. M., Eissa, I. H., Hazekamp, A., & ElSohly, M. A. (2023). Chemistry and Biological Activities of Cannflavins of the Cannabis Plant. *Cannabis and Cannabinoid Research*, *8*(6), 974–985. https://doi.org/10.1089/can.2023.0128

Abe, K., Aoki, M., Tsuji, S., Itoyama, Y., Sobue, G., Togo, M., Hamada, C., Tanaka, M., Akimoto, M., Nakamura, K., Takahashi, F., Kondo, K., Yoshino, H., Abe, K., Aoki, M., Tsuji, S., Itoyama, Y., Sobue, G., Togo, M., … Yoshino, H. (2017). Safety and efficacy of edaravone in well defined patients with amyotrophic lateral sclerosis: A randomised, double-blind, placebo-controlled trial. *The Lancet Neurology*, *16*(7), 505–512. https://doi.org/10.1016/S1474-4422(17)30115-1

Agrawal, A., Balcı, H., Hanspers, K., Coort, S. L., Martens, M., Slenter, D. N., Ehrhart, F., Digles, D., Waagmeester, A., Wassink, I., Abbassi-Daloii, T., Lopes, E. N., Iyer, A., Acosta, J. M., Willighagen, L. G., Nishida, K., Riutta, A., Basaric, H., Evelo, C. T., … Pico, A. R. (2024). WikiPathways 2024: Next generation pathway database. *Nucleic Acids Research*, *52*(D1), D679–D689. https://doi.org/10.1093/nar/gkad960

Alencar, M. A., Soares, B. L., Rangel, M. F. de A., Abdo, J. S., Almeida, R. A. P. de, Araújo, C. M. de, Souza, L. C. de, & Gomes, G. de C. (2022). Fatigue in amyotrophic lateral sclerosis and correlated factors. *Arquivos de Neuro-Psiquiatria*, *80*(10), 1045–1051. https://doi.org/10.1055/s-0042-1758563

Allada, R., Emery, P., Takahashi, J. S., & Rosbash, M. (2001). Stopping time: The genetics of fly and mouse circadian clocks. *Annual Review of Neuroscience*, *24*, 1091–1119. https://doi.org/10.1146/annurev.neuro.24.1.1091

Allnutt, A. B., Waters, A. K., Kesari, S., & Yenugonda, V. M. (2020). Physiological and Pathological Roles of Cdk5: Potential Directions for Therapeutic Targeting in Neurodegenerative Disease. *ACS Chemical Neuroscience*, *11*(9), 1218–1230. https://doi.org/10.1021/acschemneuro.0c00096

Andrews, S. (2010). *FastQC: A Quality Control tool for High Throughput Sequence Data* [Computer software]. https://www.bioinformatics.babraham.ac.uk/projects/fastqc/

Aoyama, K. (2021). Glutathione in the Brain. *International Journal of Molecular Sciences*, *22*(9), 5010. https://doi.org/10.3390/ijms22095010

Arnold, F. J., Putka, A. F., Raychaudhuri, U., Hsu, S., Bedlack, R. S., Bennett, C. L., & La Spada, A. R. (2024). Revisiting Glutamate Excitotoxicity in Amyotrophic Lateral Sclerosis and Age-Related Neurodegeneration. *International Journal of Molecular Sciences*, *25*(11), 5587. https://doi.org/10.3390/ijms25115587

Ashburner, M., Ball, C. A., Blake, J. A., Botstein, D., Butler, H., Cherry, J. M., Davis, A. P., Dolinski, K., Dwight, S. S., Eppig, J. T., Harris, M. A., Hill, D. P., Issel-Tarver, L., Kasarskis, A., Lewis, S., Matese, J. C., Richardson, J. E., Ringwald, M., Rubin, G. M., & Sherlock, G. (2000). Gene Ontology: Tool for the unification of biology. *Nature Genetics*, *25*(1), 25–29. https://doi.org/10.1038/75556

Banwait, I., Boddington, K., Soubeyrand, E., Casaretto, J., Deol, G., Karbassi, F., & Gardner, A. (2025). Transcriptomic Analysis of A Cannabis-Derived Neuroprotective Therapy in a Zebrafish Model of ALS. *ResearchHub Journal*. https://doi.org/10.55277/rhj.tv4dbb3e.7

Bass, J., & Takahashi, J. S. (2010). Circadian integration of metabolism and energetics. *Science*, *330*(6009), 1349–1354. https://doi.org/10.1126/science.1195027

Bautista, J. L., Yu, S., & Tian, L. (2021). Flavonoids in *Cannabis sativa*: Biosynthesis, Bioactivities, and Biotechnology. *ACS Omega*, *6*(8), 5119–5123. https://doi.org/10.1021/acsomega.1c00318

Benjamini, Y., & Hochberg, Y. (1995). Controlling the False Discovery Rate: A Practical and Powerful Approach to Multiple Testing. *Journal of the Royal Statistical Society: Series B (Methodological)*, *57*(1), 289–300. https://doi.org/10.1111/j.2517-6161.1995.tb02031.x

Bensimon, G., Lacomblez, L., & Meininger, V. (1994). A Controlled Trial of Riluzole in Amyotrophic Lateral Sclerosis. *New England Journal of Medicine*, *330*(9), 585–591. https://doi.org/10.1056/NEJM199403033300901

Bhardwaj, A., Bhardwaj, R., Dhawan, D. K., & Kaur, T. (2019). Exploring the Effect of Endoplasmic Reticulum Stress Inhibition by 4-Phenylbutyric Acid on AMPA-Induced Hippocampal Excitotoxicity in Rat Brain. *Neurotoxicity Research*, *35*(1), 83–91. https://doi.org/10.1007/s12640-018-9932-0

Borowicz, K., Czuczwar, S., Piskorska, B., & Banach, M. (2011). Neuroprotective Actions of Neurosteroids. *Frontiers in Endocrinology*, *2*. https://doi.org/10.3389/fendo.2011.00050

Brand, A. H., & Perrimon, N. (1993). Targeted gene expression as a means of altering cell fates and generating dominant phenotypes. *Development*, *118*(2), 401–415. https://doi.org/10.1242/dev.118.2.401

Brann, D. W., Dhandapani, K., Wakade, C., Mahesh, V. B., & Khan, M. M. (2007). Neurotrophic and neuroprotective actions of estrogen: Basic mechanisms and clinical implications. *Steroids*, *72*(5), 381–405. https://doi.org/10.1016/j.steroids.2007.02.003

Burg, T., & Van Den Bosch, L. (2025). Glycerophospholipids in ALS: Insights into disease mechanisms and clinical implication. *Molecular Neurodegeneration*, *20*(1), 85. https://doi.org/10.1186/s13024-025-00876-3

Bustamante-Barrientos, F. A., Méndez-Ruette, M., Ortloff, A., Luz-Crawford, P., Rivera, F. J., Figueroa, C. D., Molina, L., & Bátiz, L. F. (2021). The Impact of Estrogen and Estrogen-Like Molecules in Neurogenesis and Neurodegeneration: Beneficial or Harmful? *Frontiers in Cellular Neuroscience*, *15*. https://doi.org/10.3389/fncel.2021.636176

Cardona-Rossinyol, A., Mir, M., Caraballo-Miralles, V., Lladó, J., & Olmos, G. (2013). Neuroprotective Effects of Estradiol on Motoneurons in a Model of Rat Spinal Cord Embryonic Explants. *Cellular and Molecular Neurobiology*, *33*(3), 421–432. https://doi.org/10.1007/s10571-013-9908-9

Chen, J., Hu, R., Ge, H., Duanmu, W., Li, Y., Xue, X., Hu, S., & Feng, H. (2015). G-protein-coupled receptor 30-mediated antiapoptotic effect of estrogen on spinal motor

neurons following injury and its underlying mechanisms. *Molecular Medicine Reports*, *12*(2), 1733–1740. https://doi.org/10.3892/mmr.2015.3601

Choi, S. Y., Lopez-Gonzalez, R., Krishnan, G., Phillips, H. L., Li, A. N., Seeley, W. W., Yao, W.-D., Almeida, S., & Gao, F.-B. (2019). C9ORF72-ALS/FTD-associated poly(GR) binds Atp5a1 and compromises mitochondrial function in vivo. *Nature Neuroscience*, *22*(6), 851–862. https://doi.org/10.1038/s41593-019-0397-0

Conesa, A., Madrigal, P., Tarazona, S., Gomez-Cabrero, D., Cervera, A., McPherson, A., Szcześniak, M. W., Gaffney, D. J., Elo, L. L., Zhang, X., & Mortazavi, A. (2016). A survey of best practices for RNA-seq data analysis. *Genome Biology*, *17*, 13. https://doi.org/10.1186/s13059-016-0881-8

Considerations for RNA Seq read length and coverage | Illumina Knowledge. (2025, November 24). https://knowledge.illumina.com/library-preparation/rna-library-prep/library-preparation-rna-library-prep-reference_material-list/000001243

Cook, R. D. (1977). Detection of Influential Observation in Linear Regression. *Technometrics*, *19*(1), 15–18. https://doi.org/10.1080/00401706.1977.10489493

Dafinca, R., Scaber, J., Ababneh, N., Lalic, T., Weir, G., Christian, H., Vowles, J., Douglas, A. G. L., Fletcher-Jones, A., Browne, C., Nakanishi, M., Turner, M. R., Wade-Martins, R., Cowley, S. A., & Talbot, K. (2016). C9orf72 Hexanucleotide Expansions Are Associated with Altered Endoplasmic Reticulum Calcium Homeostasis and Stress Granule Formation in Induced Pluripotent Stem Cell-Derived Neurons from Patients with

Amyotrophic Lateral Sclerosis and Frontotemporal Dementia. *Stem Cells (Dayton, Ohio)*, *34*(8), 2063–2078. https://doi.org/10.1002/stem.2388

Dawadi, P., Pokharel, B., Shrestha, A., Niraula, D., Naeem, A., Miura, S., Roy, M., & Nepal, S. (2025). From bench to bytes: A practical guide to RNA sequencing data analysis. *Frontiers in Genetics*, *16*, 1697922. https://doi.org/10.3389/fgene.2025.1697922

DeJesus-Hernandez, M., Mackenzie, I. R., Boeve, B. F., Boxer, A. L., Baker, M., Rutherford, N. J., Nicholson, A. M., Finch, N. A., Flynn, H., Adamson, J., Kouri, N., Wojtas, A., Sengdy, P., Hsiung, G.-Y. R., Karydas, A., Seeley, W. W., Josephs, K. A., Coppola, G., Geschwind, D. H., … Rademakers, R. (2011). Expanded GGGGCC Hexanucleotide Repeat in Noncoding Region of C9ORF72 Causes Chromosome 9p-Linked FTD and ALS. *Neuron*, *72*(2), 245–256. https://doi.org/10.1016/j.neuron.2011.09.011

Dobin, A., Davis, C. A., Schlesinger, F., Drenkow, J., Zaleski, C., Jha, S., Batut, P., Chaisson, M., & Gingeras, T. R. (2013). STAR: Ultrafast universal RNA-seq aligner. *Bioinformatics*, *29*(1), 15–21. https://doi.org/10.1093/bioinformatics/bts635

Dobin, A., & Gingeras, T. R. (2015). Mapping RNA-seq Reads with STAR. *Current Protocols in Bioinformatics / Editoral Board, Andreas D. Baxevanis ... [et Al.]*, *51*, 11.14.1-11.14.19. https://doi.org/10.1002/0471250953.bi1114s51

Dong, X., Wang, Y., & Qin, Z. (2009). Molecular mechanisms of excitotoxicity and their relevance to pathogenesis of neurodegenerative diseases. *Acta Pharmacologica Sinica*, *30*(4), 379–387. https://doi.org/10.1038/aps.2009.24

Dorst, J., Weydt, P., Brenner, D., Witzel, S., Kandler, K., Huss, A., Herrmann, C., Wiesenfarth, M., Knehr, A., Günther, K., Müller, K., Weishaupt, J. H., Prudlo, J., Forsberg, K., Andersen, P. M., Rosenbohm, A., Schuster, J., Roselli, F., Dupuis, L., … Ludolph, A. C. (2023). Metabolic alterations precede neurofilament changes in presymptomatic ALS gene carriers. *EBioMedicine*, *90*, 104521. https://doi.org/10.1016/j.ebiom.2023.104521

Drosophila_melanogaster—Ensembl genome browser 113. (2024, October). https://oct2024.archive.ensembl.org/Drosophila_melanogaster/Info/Index

Eggers, C., Fujitani, M., Kato, R., & Smid, S. (2019). Novel cannabis flavonoid, cannflavin A displays both a hormetic and neuroprotective profile against amyloid β-mediated neurotoxicity in PC12 cells: Comparison with geranylated flavonoids, mimulone and diplacone. *Biochemical Pharmacology*, *169*, 113609. https://doi.org/10.1016/j.bcp.2019.08.011

Fang, Z., Liu, X., & Peltz, G. (2023). GSEApy: A comprehensive package for performing gene set enrichment analysis in Python. *Bioinformatics*, *39*(1), btac757. https://doi.org/10.1093/bioinformatics/btac757

Fehér, Á., Giricz, Z., Juhász, A., Pákáski, M., Janka, Z., & Kálmán, J. (2018). ABCA1 rs2230805 and rs2230806 common gene variants are associated with Alzheimer's disease. *Neuroscience Letters*, *664*, 79–83. https://doi.org/10.1016/j.neulet.2017.11.027

Gao, S., & Hu, M. (2010). Bioavailability Challenges Associated with Development of Anti-Cancer Phenolics. *Mini Reviews in Medicinal Chemistry*, *10*(6), 550–567. https://doi.org/10.2174/138955710791384081

Garcia-Segura, L. M., & Balthazart, J. (2009). Steroids and neuroprotection: New advances. *Frontiers in Neuroendocrinology, Steroids and Neuroprotection*, *30*(2), v–ix. https://doi.org/10.1016/j.yfrne.2009.04.006

Gerstner, J. R., Flores, C. C., Lefton, M., Rogers, B., & Davis, C. J. (2023). FABP7: A glial integrator of sleep, circadian rhythms, plasticity, and metabolic function. *Frontiers in Systems Neuroscience*, *17*, 1212213. https://doi.org/10.3389/fnsys.2023.1212213

Grassano, M., Moglia, C., Palumbo, F., Koumantakis, E., Cugnasco, P., Callegaro, S., Canosa, A., Manera, U., Vasta, R., De Mattei, F., Matteoni, E., Fuda, G., Salamone, P., Marchese, G., Casale, F., De Marchi, F., Mazzini, L., Mora, G., Calvo, A., & Chiò, A. (2024). Sex Differences in Amyotrophic Lateral Sclerosis Survival and Progression: A Multidimensional Analysis. *Annals of Neurology*, *96*(1), 159–169. https://doi.org/10.1002/ana.26933

Graveley, B. R., Brooks, A. N., Carlson, J. W., Duff, M. O., Landolin, J. M., Yang, L., Artieri, C. G., van Baren, M. J., Boley, N., Booth, B. W., Brown, J. B., Cherbas, L., Davis, C. A., Dobin, A., Li, R., Lin, W., Malone, J. H., Mattiuzzo, N. R., Miller, D., … Celniker, S. E. (2011). The developmental transcriptome of Drosophila melanogaster. *Nature*, *471*(7339), 473–479. https://doi.org/10.1038/nature09715

Hardiman, O., Al-Chalabi, A., Chio, A., Corr, E. M., Logroscino, G., Robberecht, W., Shaw, P. J., Simmons, Z., & Van Den Berg, L. H. (2017). Amyotrophic lateral sclerosis. *Nature Reviews Disease Primers*, *3*(1), 17071. https://doi.org/10.1038/nrdp.2017.71

Hegde, K. N., & Srivastava, A. (2022). Drosophila melanogaster as a Tool for Amyotrophic Lateral Sclerosis Research. *Journal of Developmental Biology*, *10*(3), 36. https://doi.org/10.3390/jdb10030036

Hu, M. (2007). Commentary: Bioavailability of flavonoids and polyphenols: call to arms. *Molecular Pharmaceutics*, *4*(6), 803–806. https://doi.org/10.1021/mp7001363

Ichinose, T., Yu, S., Wang, X. Q., & Yu, S. P. (2003). Ca2+-independent, but voltage- and activity-dependent regulation of the NMDA receptor outward K+ current in mouse cortical neurons. *The Journal of Physiology*, *551*(Pt 2), 403–417. https://doi.org/10.1113/jphysiol.2003.041723

Josephy, D. P., Guengerich, P. F., & Miners, J. O. (2005). "Phase I and Phase II" Drug Metabolism: Terminology that we Should Phase Out? *Drug Metabolism Reviews*, *37*(4), 575–580. https://doi.org/10.1080/03602530500251220

Kanehisa, M. (2019). Toward understanding the origin and evolution of cellular organisms. *Protein Science: A Publication of the Protein Society*, *28*(11), 1947–1951. https://doi.org/10.1002/pro.3715

Kanehisa, M., Furumichi, M., Sato, Y., Matsuura, Y., & Ishiguro-Watanabe, M. (2025). KEGG: Biological systems database as a model of the real world. *Nucleic Acids Research*, *53*(D1), D672–D677. https://doi.org/10.1093/nar/gkae909

Kanehisa, M., & Goto, S. (2000). KEGG: Kyoto encyclopedia of genes and genomes. *Nucleic Acids Research*, *28*(1), 27–30. https://doi.org/10.1093/nar/28.1.27

Kemp, S., Theodoulou, F. L., & Wanders, R. J. (2011). Mammalian peroxisomal ABC transporters: From endogenous substrates to pathology and clinical significance. *British Journal of Pharmacology*, *164*(7), 1753–1766. https://doi.org/10.1111/j.1476-5381.2011.01435.x

Koldamova, R., Fitz, N. F., & Lefterov, I. (2014). ATP-binding cassette transporter A1: From metabolism to neurodegeneration. *Neurobiology of Disease, Special Issue: Metabolic Disorders and Neurodegeneration*, *72*, 13–21. https://doi.org/10.1016/j.nbd.2014.05.007

Kölsch, H., Linnebank, M., Lütjohann, D., Jessen, F., Wüllner, U., Harbrecht, U., Thelen, K. M., Kreis, M., Hentschel, F., Schulz, A., Von Bergmann, K., Maier, W., & Heun, R. (2004). Polymorphisms in glutathione S-transferase omega-1 and AD, vascular dementia, and stroke. *Neurology*, *63*(12), 2255–2260. https://doi.org/10.1212/01.WNL.0000147294.29309.47

Konakchieva, R., Mladenov, M., Konaktchieva, M., Sazdova, I., Gagov, H., & Nikolaev, G. (2025). Circadian Clock Deregulation and Metabolic Reprogramming: A System Biology Approach to Tissue-Specific Redox Signaling and Disease Development. *International Journal of Molecular Sciences*, *26*(13), 6267. https://doi.org/10.3390/ijms26136267

Kotlyarov, S., & Kotlyarova, A. (2021). The Role of ABC Transporters in Lipid Metabolism and the Comorbid Course of Chronic Obstructive Pulmonary Disease and Atherosclerosis. *International Journal of Molecular Sciences*, *22*(13), 6711. https://doi.org/10.3390/ijms22136711

Lambert, J. D., Hong, J., Kim, D. H., Mishin, V. M., & Yang, C. S. (2004). Piperine Enhances the Bioavailability of the Tea Polyphenol (−)-Epigallocatechin-3-gallate in Mice. *The Journal of Nutrition*, *134*(8), 1948–1952. https://doi.org/10.1093/jn/134.8.1948

Lang, C. (2025). Sleep alterations in amyotrophic lateral sclerosis. *Current Opinion in Neurology*, *38*(5), 606–613. https://doi.org/10.1097/WCO.0000000000001424

Langfelder, P., & Horvath, S. (2008). WGCNA: An R package for weighted correlation network analysis. *BMC Bioinformatics*, *9*, 559. https://doi.org/10.1186/1471-2105-9-559

Larkin, A., Marygold, S. J., Antonazzo, G., Attrill, H., dos Santos, G., Garapati, P. V., Goodman, J. L., Gramates, L. S., Millburn, G., Strelets, V. B., Tabone, C. J., Thurmond, J., FlyBase Consortium, Perrimon, N., Gelbart, S. R., Agapite, J., Broll, K., Crosby, M., Dos Santos, G., … Lovato, T. (2021). FlyBase: Updates to the *Drosophila melanogaster* knowledge base. *Nucleic Acids Research*, *49*(D1), D899–D907. https://doi.org/10.1093/nar/gkaa1026

Leys, C., Ley, C., Klein, O., Bernard, P., & Licata, L. (2013). Detecting outliers: Do not use standard deviation around the mean, use absolute deviation around the median. *Journal of Experimental Social Psychology*, *49*(4), 764–766. https://doi.org/10.1016/j.jesp.2013.03.013

Li, Y.-J., Oliveira, S. A., Xu, P., Martin, E. R., Stenger, J. E., Scherzer, C. R., Hauser, M. A., Scott, W. K., Small, G. W., Nance, M. A., Watts, R. L., Hubble, J. P., Koller, W. C., Pahwa, R., Stern, M. B., Hiner, B. C., Jankovic, J., Goetz, C. G., Mastaglia, F., … Pericak-Vance, M. A. (2003). Glutathione S-transferase omega-1 modifies age-at-onset of

Alzheimer disease and Parkinson disease. *Human Molecular Genetics*, *12*(24), 3259–3267. https://doi.org/10.1093/hmg/ddg357

Liu, Z., & Hu, M. (2007). Natural Polyphenol Disposition via Coupled Metabolic Pathways. *Expert Opinion on Drug Metabolism & Toxicology*, *3*(3), 389–406. https://doi.org/10.1517/17425255.3.3.389

Lopez-Gonzalez, R., Lu, Y., Gendron, T. F., Karydas, A., Tran, H., Yang, D., Petrucelli, L., Miller, B. L., Almeida, S., & Gao, F.-B. (2016). Poly(GR) in C9ORF72-Related ALS/FTD Compromises Mitochondrial Function and Increases Oxidative Stress and DNA Damage in iPSC-Derived Motor Neurons. *Neuron*, *92*(2), 383–391. https://doi.org/10.1016/j.neuron.2016.09.015

Love, M. I., Huber, W., & Anders, S. (2014). Moderated estimation of fold change and dispersion for RNA-seq data with DESeq2. *Genome Biology*, *15*(12), 550. https://doi.org/10.1186/s13059-014-0550-8

Ma, S., & Dai, Y. (2011). Principal component analysis based methods in bioinformatics studies. *Briefings in Bioinformatics*, *12*(6), 714–722. https://doi.org/10.1093/bib/bbq090

Majounie, E., Renton, A. E., Mok, K., Dopper, E. G., Waite, A., Rollinson, S., Chiò, A., Restagno, G., Nicolaou, N., Simon-Sanchez, J., Van Swieten, J. C., Abramzon, Y., Johnson, J. O., Sendtner, M., Pamphlett, R., Orrell, R. W., Mead, S., Sidle, K. C., Houlden, H., … Traynor, B. J. (2012). Frequency of the C9orf72 hexanucleotide repeat expansion in patients with amyotrophic lateral sclerosis and frontotemporal dementia: A

cross-sectional study. *The Lancet Neurology*, *11*(4), 323–330. https://doi.org/10.1016/S1474-4422(12)70043-1

Martin, M. (2011). Cutadapt removes adapter sequences from high-throughput sequencing reads. *EMBnet.Journal*, *17*(1), 10. https://doi.org/10.14806/ej.17.1.200

Maruyama, T., Tanabe, S., Uyeda, A., Suzuki, T., & Muramatsu, R. (2023). Free fatty acids support oligodendrocyte survival in a mouse model of amyotrophic lateral sclerosis. *Frontiers in Cellular Neuroscience*, *17*, 1081190. https://doi.org/10.3389/fncel.2023.1081190

McKee, C. A., Polino, A. J., King, M. W., & Musiek, E. S. (2023). Circadian clock protein BMAL1 broadly influences autophagy and endolysosomal function in astrocytes. *Proceedings of the National Academy of Sciences of the United States of America*, *120*(20), e2220551120. https://doi.org/10.1073/pnas.2220551120

Menon, P., Geevasinga, N., van den Bos, M., Yiannikas, C., Kiernan, M. C., & Vucic, S. (2017). Cortical hyperexcitability and disease spread in amyotrophic lateral sclerosis. *European Journal of Neurology*, *24*(6), 816–824. https://doi.org/10.1111/ene.13295

Milacic, M., Beavers, D., Conley, P., Gong, C., Gillespie, M., Griss, J., Haw, R., Jassal, B., Matthews, L., May, B., Petryszak, R., Ragueneau, E., Rothfels, K., Sevilla, C., Shamovsky, V., Stephan, R., Tiwari, K., Varusai, T., Weiser, J., … D'Eustachio, P. (2024). The Reactome Pathway Knowledgebase 2024. *Nucleic Acids Research*, *52*(D1), D672–D678. https://doi.org/10.1093/nar/gkad1025

Miller, J. (1991). Short Report: Reaction Time Analysis with Outlier Exclusion: Bias Varies with Sample Size. *The Quarterly Journal of Experimental Psychology Section A*, *43*(4), 907–912. https://doi.org/10.1080/14640749108400962

Miller, R. G., Mitchell, J. D., & Moore, D. H. (2012). Riluzole for amyotrophic lateral sclerosis (ALS)/motor neuron disease (MND). *Cochrane Database of Systematic Reviews*, *2012*(3). https://doi.org/10.1002/14651858.CD001447.pub3

Milling, S. (2020). It's time to think about circadian rhythms. *Immunology*, *161*(4), 259–260. https://doi.org/10.1111/imm.13284

Mizielinska, S., Grönke, S., Niccoli, T., Ridler, C. E., Clayton, E. L., Devoy, A., Moens, T., Norona, F. E., Woollacott, I. O. C., Pietrzyk, J., Cleverley, K., Nicoll, A. J., Pickering-Brown, S., Dols, J., Cabecinha, M., Hendrich, O., Fratta, P., Fisher, E. M. C., Partridge, L., & Isaacs, A. M. (2014). *C9orf72* repeat expansions cause neurodegeneration in *Drosophila* through arginine-rich proteins. *Science*, *345*(6201), 1192–1194. https://doi.org/10.1126/science.1256800

Muzellec, B., Teleńczuk, M., Cabeli, V., & Andreux, M. (2023). PyDESeq2: A python package for bulk RNA-seq differential expression analysis. *Bioinformatics (Oxford, England)*, *39*(9), btad547. https://doi.org/10.1093/bioinformatics/btad547

Nakamura, R., Kurihara, M., Ogawa, N., Kitamura, A., Yamakawa, I., Bamba, S., Sanada, M., Sasaki, M., & Urushitani, M. (2021). Prognostic prediction by hypermetabolism varies depending on the nutritional status in early amyotrophic lateral sclerosis. *Scientific Reports*, *11*(1), 17943. https://doi.org/10.1038/s41598-021-97196-5

Nissbrandt, H., Bergquist, F., Jonason, J., & Engberg, G. (2001). Inhibition of cytochrome P450 2E1 induces an increase in extracellular dopamine in rat substantia nigra: A new metabolic pathway? *Synapse*, *40*(4), 294–301. https://doi.org/10.1002/syn.1052

O'Leary, T., Williams, A. H., Franci, A., & Marder, E. (2014). Cell types, network homeostasis, and pathological compensation from a biologically plausible ion channel expression model. *Neuron*, *82*(4), 809–821. https://doi.org/10.1016/j.neuron.2014.04.002

O'Neil, D., Glowatz, H., & Schlumpberger, M. (2013). Ribosomal RNA depletion for efficient use of RNA-seq capacity. *Current Protocols in Molecular Biology*, *Chapter 4*, Unit 4.19. https://doi.org/10.1002/0471142727.mb0419s103

Onesto, E., Colombrita, C., Gumina, V., Borghi, M. O., Dusi, S., Doretti, A., Fagiolari, G., Invernizzi, F., Moggio, M., Tiranti, V., Silani, V., & Ratti, A. (2016). Gene-specific mitochondria dysfunctions in human TARDBP and C9ORF72 fibroblasts. *Acta Neuropathologica Communications*, *4*(1), 47. https://doi.org/10.1186/s40478-016-0316-5

Ouzzine, M., Gulberti, S., Ramalanjaona, N., Magdalou, J., & Fournel-Gigleux, S. (2014). The UDP-glucuronosyltransferases of the blood-brain barrier: Their role in drug metabolism and detoxication. *Frontiers in Cellular Neuroscience*, *8*. https://doi.org/10.3389/fncel.2014.00349

Paganoni, S., Macklin, E. A., Hendrix, S., Berry, J. D., Elliott, M. A., Maiser, S., Karam, C., Caress, J. B., Owegi, M. A., Quick, A., Wymer, J., Goutman, S. A., Heitzman, D., Heiman-Patterson, T., Jackson, C. E., Quinn, C., Rothstein, J. D., Kasarskis, E. J., Katz, J., … Cudkowicz, M. E. (2020). Trial of Sodium Phenylbutyrate–Taurursodiol for

Amyotrophic Lateral Sclerosis. *New England Journal of Medicine*, *383*(10), 919–930. https://doi.org/10.1056/NEJMoa1916945

Parisi, M., Nuttall, R., Naiman, D., Bouffard, G., Malley, J., Andrews, J., Eastman, S., & Oliver, B. (2003). Paucity of genes on the Drosophila X chromosome showing male-biased expression. *Science*, *299*(5607), 697–700. https://doi.org/10.1126/science.1079190

Petrenko, V., Sinturel, F., Riezman, H., & Dibner, C. (2023). Lipid metabolism around the body clocks. *Progress in Lipid Research*, *91*, 101235. https://doi.org/10.1016/j.plipres.2023.101235

Pharaoh, G., Sataranatarajan, K., Street, K., Hill, S., Gregston, J., Ahn, B., Kinter, C., Kinter, M., & Van Remmen, H. (2019). Metabolic and Stress Response Changes Precede Disease Onset in the Spinal Cord of Mutant SOD1 ALS Mice. *Frontiers in Neuroscience*, *13*, 487. https://doi.org/10.3389/fnins.2019.00487

Philips, T., & Robberecht, W. (2011). Neuroinflammation in amyotrophic lateral sclerosis: Role of glial activation in motor neuron disease. *The Lancet Neurology*, *10*(3), 253–263. https://doi.org/10.1016/S1474-4422(11)70015-1

Phillips, M. C. L., Johnston, S. E., Simpson, P., Chang, D. K., Mather, D., & Dick, R. J. (2024). Time-restricted ketogenic diet in amyotrophic lateral sclerosis: A case study. *Frontiers in Neurology*, *14*, 1329541. https://doi.org/10.3389/fneur.2023.1329541

Puig-Bosch, X., Ballmann, M., Bieletzki, S., Antkowiak, B., Rudolph, U., Zeilhofer, H. U., & Rammes, G. (2023). Neurosteroids Mediate Neuroprotection in an In Vitro Model of

Hypoxic/Hypoglycaemic Excitotoxicity via δ-GABAA Receptors without Affecting Synaptic Plasticity. *International Journal of Molecular Sciences*, *24*(10). https://doi.org/10.3390/ijms24109056

Rea, K. A., Casaretto, J. A., Al-Abdul-Wahid, M. S., Sukumaran, A., Geddes-McAlister, J., Rothstein, S. J., & Akhtar, T. A. (2019). Biosynthesis of cannflavins A and B from *Cannabis sativa* L. *Phytochemistry*, *164*, 162–171. https://doi.org/10.1016/j.phytochem.2019.05.009

Renton, A. E., Majounie, E., Waite, A., Simón-Sánchez, J., Rollinson, S., Gibbs, J. R., Schymick, J. C., Laaksovirta, H., van Swieten, J. C., Myllykangas, L., Kalimo, H., Paetau, A., Abramzon, Y., Remes, A. M., Kaganovich, A., Scholz, S. W., Duckworth, J., Ding, J., Harmer, D. W., … Traynor, B. J. (2011). A Hexanucleotide Repeat Expansion in C9ORF72 Is the Cause of Chromosome 9p21-Linked ALS-FTD. *Neuron*, *72*(2), 257–268. https://doi.org/10.1016/j.neuron.2011.09.010

Rosati, D., Palmieri, M., Brunelli, G., Morrione, A., Iannelli, F., Frullanti, E., & Giordano, A. (2024). Differential gene expression analysis pipelines and bioinformatic tools for the identification of specific biomarkers: A review. *Computational and Structural Biotechnology Journal*, *23*, 1154–1168. https://doi.org/10.1016/j.csbj.2024.02.018

Salvatori, I., Ferri, A., Scaricamazza, S., Giovannelli, I., Serrano, A., Rossi, S., D'Ambrosi, N., Cozzolino, M., Giulio, A. D., Moreno, S., Valle, C., & Carrì, M. T. (2018). Differential toxicity of TAR DNA-binding protein 43 isoforms depends on their submitochondrial

localization in neuronal cells. *Journal of Neurochemistry*, *146*(5), 585–597. https://doi.org/10.1111/jnc.14465

Schulz, J. A., Hartz, A. M. S., & Bauer, B. (2023). ABCB1 and ABCG2 Regulation at the Blood-Brain Barrier: Potential New Targets to Improve Brain Drug Delivery. *Pharmacological Reviews*, *75*(5), 815–853. https://doi.org/10.1124/pharmrev.120.000025

Seyfried, T. N., Shelton, L., Arismendi-Morillo, G., Kalamian, M., Elsakka, A., Maroon, J., & Mukherjee, P. (2019). Provocative Question: Should Ketogenic Metabolic Therapy Become the Standard of Care for Glioblastoma? *Neurochemical Research*, *44*(10), 2392–2404. https://doi.org/10.1007/s11064-019-02795-4

Shen, S., Callaghan, D., Juzwik, C., Xiong, H., Huang, P., & Zhang, W. (2010). ABCG2 reduces ROS-mediated toxicity and inflammation: A potential role in Alzheimer's disease. *Journal of Neurochemistry*, *114*(6), 1590–1604. https://doi.org/10.1111/j.1471-4159.2010.06887.x

Sheng, Y., Yang, H., Wu, T., Zhu, L., Liu, L., & Liu, X. (2021). Alterations of Cytochrome P450s and UDP-Glucuronosyltransferases in Brain Under Diseases and Their Clinical Significances. *Frontiers in Pharmacology*, *12*. https://doi.org/10.3389/fphar.2021.650027

Shoba, G., Joy, D., Joseph, T., Majeed, M., Rajendran, R., & Srinivas, P. (1998). Influence of Piperine on the Pharmacokinetics of Curcumin in Animals and Human Volunteers. *Planta Medica*, *64*(04), 353–356. https://doi.org/10.1055/s-2006-957450

Silva-Adaya, D., Garza-Lombó, C., & Gonsebatt, M. E. (2021). Xenobiotic transport and metabolism in the human brain. *NeuroToxicology*, *86*, 125–138. https://doi.org/10.1016/j.neuro.2021.08.004

Stasiłowicz-Krzemień, A., Nogalska, W., Maszewska, Z., Maleszka, M., Dobroń, M., Szary, A., Kępa, A., Żarowski, M., Hojan, K., Lukowicz, M., & Cielecka-Piontek, J. (2024). The Use of Compounds Derived from Cannabis sativa in the Treatment of Epilepsy, Painful Conditions, and Neuropsychiatric and Neurodegenerative Disorders. *International Journal of Molecular Sciences*, *25*(11), 5749. https://doi.org/10.3390/ijms25115749

Sun, K., Chang, K., Clawson, S., Ghosh, S., Mirzaei, H., Regnier, F., & Shah, K. (2011). Glutathione-S-transferase P1 is a critical regulator of Cdk5 kinase activity. *Journal of Neurochemistry*, *118*(5), 902–914. https://doi.org/10.1111/j.1471-4159.2011.07343.x

Szklarczyk, D., Kirsch, R., Koutrouli, M., Nastou, K., Mehryary, F., Hachilif, R., Gable, A. L., Fang, T., Doncheva, N. T., Pyysalo, S., Bork, P., Jensen, L. J., & von Mering, C. (2023). The STRING database in 2023: Protein-protein association networks and functional enrichment analyses for any sequenced genome of interest. *Nucleic Acids Research*, *51*(D1), D638–D646. https://doi.org/10.1093/nar/gkac1000

Tarling, E. J., de Aguiar Vallim, T. Q., & Edwards, P. A. (2013). Role of ABC transporters in lipid transport and human disease. *Trends in Endocrinology and Metabolism: TEM*, *24*(7), 342–350. https://doi.org/10.1016/j.tem.2013.01.006

Taylor, J. P., Brown, R. H., & Cleveland, D. W. (2016). Decoding ALS: From genes to mechanism. *Nature*, *539*(7628), 197–206. https://doi.org/10.1038/nature20413

The Gene Ontology Consortium. (2026). The Gene Ontology knowledgebase in 2026. *Nucleic Acids Research*, *54*(D1), D1779–D1792. https://doi.org/10.1093/nar/gkaf1292

Turrigiano, G. (2012). Homeostatic synaptic plasticity: Local and global mechanisms for stabilizing neuronal function. *Cold Spring Harbor Perspectives in Biology*, *4*(1), a005736. https://doi.org/10.1101/cshperspect.a005736

Van De Giessen, E., Fogh, I., Gopinath, S., Smith, B., Hu, X., Powell, J., Andersen, P., Nicholson, G., Al Chalabi, A., & Shaw, C. E. (2008). Association study on glutathione S-transferase omega 1 and 2 and familial ALS. *Amyotrophic Lateral Sclerosis*, *9*(2), 81–84. https://doi.org/10.1080/17482960701702553

Van Den Bosch, L., Van Damme, P., Bogaert, E., & Robberecht, W. (2006). The role of excitotoxicity in the pathogenesis of amyotrophic lateral sclerosis. *Biochimica et Biophysica Acta (BBA) - Molecular Basis of Disease, Molecular Basis of Amyotrophic Lateral Sclerosis*, *1762*(11), 1068–1082. https://doi.org/10.1016/j.bbadis.2006.05.002

Vandoorne, T., De Bock, K., & Van Den Bosch, L. (2018). Energy metabolism in ALS: An underappreciated opportunity? *Acta Neuropathologica*, *135*(4), 489–509. https://doi.org/10.1007/s00401-018-1835-x

Veech, R. L. (2004). The therapeutic implications of ketone bodies: The effects of ketone bodies in pathological conditions: ketosis, ketogenic diet, redox states, insulin resistance, and mitochondrial metabolism. *Prostaglandins, Leukotrienes and Essential Fatty Acids, Metabolic and Health Implications of Moderate Ketosis and the Ket Ogenic Diet*, *70*(3), 309–319. https://doi.org/10.1016/j.plefa.2003.09.007

Villa, M., Wu, J., Hansen, S., & Pahnke, J. (2024). Emerging Role of ABC Transporters in Glia Cells in Health and Diseases of the Central Nervous System. *Cells*, *13*(9), 740. https://doi.org/10.3390/cells13090740

Wainger, B. J., Kiskinis, E., Mellin, C., Wiskow, O., Han, S. S. W., Sandoe, J., Perez, N. P., Williams, L. A., Lee, S., Boulting, G., Berry, J. D., Brown, R. H., Cudkowicz, M. E., Bean, B. P., Eggan, K., & Woolf, C. J. (2014). Intrinsic membrane hyperexcitability of amyotrophic lateral sclerosis patient-derived motor neurons. *Cell Reports*, *7*(1), 1–11. https://doi.org/10.1016/j.celrep.2014.03.019

Wainger, B. J., Macklin, E. A., Vucic, S., McIlduff, C. E., Paganoni, S., Maragakis, N. J., Bedlack, R., Goyal, N. A., Rutkove, S. B., Lange, D. J., Rivner, M. H., Goutman, S. A., Ladha, S. S., Mauricio, E. A., Baloh, R. H., Simmons, Z., Pothier, L., Kassis, S. B., La, T., … Cudkowicz, M. E. (2021). Effect of Ezogabine on Cortical and Spinal Motor Neuron Excitability in Amyotrophic Lateral Sclerosis: A Randomized Clinical Trial. *JAMA Neurology*, *78*(2), 186–196. https://doi.org/10.1001/jamaneurol.2020.4300

Wanders, R. J. A., & Waterham, H. R. (2006). Biochemistry of mammalian peroxisomes revisited. *Annual Review of Biochemistry*, *75*, 295–332. https://doi.org/10.1146/annurev.biochem.74.082803.133329

Wang, P., Deng, J., Dong, J., Liu, J., Bigio, E. H., Mesulam, M., Wang, T., Sun, L., Wang, L., Lee, A. Y.-L., McGee, W. A., Chen, X., Fushimi, K., Zhu, L., & Wu, J. Y. (2019). TDP-43 induces mitochondrial damage and activates the mitochondrial unfolded protein response. *PLoS Genetics*, *15*(5), e1007947. https://doi.org/10.1371/journal.pgen.1007947

Wang, W., Wang, L., Lu, J., Siedlak, S. L., Fujioka, H., Liang, J., Jiang, S., Ma, X., Jiang, Z., da Rocha, E. L., Sheng, M., Choi, H., Lerou, P. H., Li, H., & Wang, X. (2016). The inhibition of TDP-43 mitochondrial localization blocks its neuronal toxicity. *Nature Medicine*, *22*(8), 869–878. https://doi.org/10.1038/nm.4130

Wang, X., Xu, Z., Cai, Y., Zeng, S., Peng, B., Ren, X., Yan, Y., & Gong, Z. (2020). Rheostatic Balance of Circadian Rhythm and Autophagy in Metabolism and Disease. *Frontiers in Cell and Developmental Biology*, *8*, 616434. https://doi.org/10.3389/fcell.2020.616434

Werz, O., Seegers, J., Schaible, A. M., Weinigel, C., Barz, D., Koeberle, A., Allegrone, G., Pollastro, F., Zampieri, L., Grassi, G., & Appendino, G. (2014). Cannflavins from hemp sprouts, a novel cannabinoid-free hemp food product, target microsomal prostaglandin E2 synthase-1 and 5-lipoxygenase. *PharmaNutrition*, *2*(3), 53–60. https://doi.org/10.1016/j.phanu.2014.05.001

Weskamp, K., Tank, E. M., Miguez, R., McBride, J. P., Gómez, N. B., White, M., Lin, Z., Gonzalez, C. M., Serio, A., Sreedharan, J., & Barmada, S. J. (2020). Shortened TDP43 isoforms upregulated by neuronal hyperactivity drive TDP43 pathology in ALS. *The Journal of Clinical Investigation*, *130*(3), 1139. https://doi.org/10.1172/JCI130988

Xu, W., & Xu, J. (2018). C9orf72 Dipeptide Repeats Cause Selective Neurodegeneration and Cell-Autonomous Excitotoxicity in Drosophila Glutamatergic Neurons. *The Journal of Neuroscience: The Official Journal of the Society for Neuroscience*, *38*(35), 7741–7752. https://doi.org/10.1523/JNEUROSCI.0908-18.2018

Yan, Y., Maisenbacher, M., Huang, C., & Fan, S. (2025). Detoxification and age-related neurodegenerative diseases: Correlation and therapeutic potential. *Pharmacological Research*, *218*, 107849. https://doi.org/10.1016/j.phrs.2025.107849

Yang, G., Ge, S., Singh, R., Basu, S., Shatzer, K., Zen, M., Liu, J., Tu, Y., Zhang, C., Wei, J., Shi, J., Zhu, L., Liu, Z., Wang, Y., Gao, S., & Hu, M. (2017). Glucuronidation: Driving Factors and Their Impact on Glucuronide Disposition. *Drug Metabolism Reviews*, *49*(2), 105–138. https://doi.org/10.1080/03602532.2017.1293682

Zamani, A., Thomas, E., & Wright, D. K. (2024). Sex biology in amyotrophic lateral sclerosis. *Ageing Research Reviews*, *95*, 102228. https://doi.org/10.1016/j.arr.2024.102228

Zhang, M., Rottschäfer, V., & C. M. De Lange, E. (2024). The potential impact of CYP and UGT drug-metabolizing enzymes on brain target site drug exposure. *Drug Metabolism Reviews*, *56*(1), 1–30. https://doi.org/10.1080/03602532.2023.2297154

Zhang, W., Zhang, L., Liang, B., Schroeder, D., Zhang, Z., Cox, G. A., Li, Y., & Lin, D.-T. (2016). Hyperactive somatostatin interneurons contribute to excitotoxicity in neurodegenerative disorders. *Nature Neuroscience*, *19*(4), 557–559. https://doi.org/10.1038/nn.4257

Zhou, Z. D., Yi, L. X., Wang, D. Q., Lim, T. M., & Tan, E. K. (2023). Role of dopamine in the pathophysiology of Parkinson's disease. *Translational Neurodegeneration*, *12*(1), 44. https://doi.org/10.1186/s40035-023-00378-6

Zhu, A., Ibrahim, J. G., & Love, M. I. (2019). Heavy-tailed prior distributions for sequence count data: Removing the noise and preserving large differences. *Bioinformatics (Oxford, England)*, *35*(12), 2084–2092. https://doi.org/10.1093/bioinformatics/bty895